이학박사학위논문

오토파지와 리소좀 유전자 조절 과정에서 USF2와 TFEB 간의 경쟁적 메커니즘에 대한 연구

Studies on the competitive mechanisms between USF2 and TFEB in the regulation of autophagy and lysosomal genes

2025년 2월

서울대학교 대학원

생명과학부

김 재 범

오토파지와 리소좀 유전자 조절 과정에서 **USF2**와 **TFEB** 간의 경쟁적 메커니즘에 대한 연구

Studies on the competitive mechanisms between USF2 and TFEB in the regulation of autophagy and lysosomal genes

지도교수 백 성 희

이 논문을 이학박사 학위논문으로 제출함

2024년 12월

서울대학교 대학원

생명과학부

김 재 범

김재범의 박사 학위논문을 인준함

2024년 12월

위 원 장 김 종 서 (인)

부위원장 백 성 희 (인)

위 원 김 근 일 (인)

위 원 김 익 수 (인)

위 원 장 원 열 (인)

Studies on the competitive mechanisms between USF2 and TFEB in the regulation of autophagy and lysosomal genes

by

Jaebeom Kim

Advisor

Professor Sung Hee Baek, Ph.D.

A Thesis for the Degree of Doctor of Philosophy

February 2025

School of Biological Sciences
Seoul National University

ABSTRACT

Jaebeom Kim

School of Biological Sciences

The Graduate School

Seoul National University

Autophagy, a highly conserved self-digestion, is triggered by various environmental signals, including nutrient scarcity. The regulation of lysosomal and autophagy-related processes is pivotal to maintaining cellular homeostasis and basal metabolism. The consequences of disrupting or diminishing lysosomal and autophagy systems have been investigated; however, information on the implications of hyperactivating lysosomal and autophagy genes on homeostasis is limited. Here, I present a mechanism of transcriptional repression involving upstream stimulatory factor 2 (USF2), which inhibits lysosomal and autophagy genes under nutrient-rich conditions. I find that USF2, together with HDAC1, binds to the CLEAR motif within lysosomal genes, thereby diminishing histone H3K27 acetylation, restricting chromatin accessibility, and downregulating lysosomal gene expression. Under starvation, USF2 competes with transcription factor EB (TFEB),

a master transcriptional activator of lysosomal and autophagy genes, to bind to target gene promoters in a phosphorylation-dependent manner. The GSK3β-mediated phosphorylation of the USF2 S155 site governs USF2 DNA-binding activity, which is involved in lysosomal gene repression. These findings have potential applications in the treatment of protein aggregation-associated diseases, including α1-antitrypsin deficiency. Notably, USF2 repression is a promising therapeutic strategy for lysosomal and autophagy-related diseases.

Keywords

USF2, Autophagy, Lysosome, Nucleosome Remodeling and Deacetylase Complex (NuRD), Histone 3 Lysine 27 Acetylation (H3K27Ac), TFEB, Post-Translational Modification (PTM), a1-AntiTrypsin Deficiency (AATD)

Student Number: 2016-20380

CONTENTS

	Page
ABSTRACT	**i**
CONTENTS	**iii**
LIST OF FIGURES AND TABLES	**vi**
CHAPTER I. Introduction	**1**
I-1. Autophagy	**2**
I.1. General information about autophagy	2
1.2. Transcriptional and epigenetic regulation of autophagy	4
I-2. USF2	**5**
2.1. General information about USF2	5
2.2. The structure of USF2	6
2.3. Phosphorylation of USF2	8
I-3. NuRD complex	**10**

3.1. General information about NuRD complex 10

3.2. Repressive mechanism of NuRD complex deacetylating H3K27Ac 11

I-4. α1-antitrypsin deficiency (AATD) disease 12

4.1. Causes of AATD 12

4.2. Therapeutic approach of AATD 13

CHAPTER II. USF2 Represses Autophagy and Lysosome Biogenesis Through Epigenetic Mechanisms With the NuRD Complex 15

II-1. Summary 16

II-2. Introduction 17

II-3. Results 19

II-4. Discussion 44

II-5. Materials and Methods 47

CHAPTER III. USF2 Competes With TFEB to Regulate Autophagy and Lysosome Genes and application to α1-Antitrypsin Deficiency **57**

III-1. Summary **58**

III-2. Introduction **60**

III-3. Results **62**

III-4. Discussion **84**

III-5. Materials and Methods **88**

CHAPTER IV. Conclusion **96**

REFERENCES **100**

국문 초록 / ABSTRACT IN KOREAN **107**

LIST OF FIGURES AND TABLES

Figure I-1. Diagrammatic illustration of the autophagy process

Figure I-2. Diagrammatic illustration of USF2 structure

Figure I-3. Diagrammatic illustration of USF2 phosphorylation

Figure I-4. Diagrammatic illustration of the degradation of ATZ aggregates

Figure II-1. USF2 as a key transcription factor in lysosomal gene regulation identified through ChIP-seq analysis

Figure II-2. USF2 knockdown enhances lysosomal biogenesis

Figure II-3. Generation and characterization of *Usf2*$^{-/-}$ mice revealing embryonic lethality

Figure II-4. Loss of USF2 enhances lysosomal biogenesis and proteolytic activity in MEFs

Figure II-5. USF2 reconstitution restores lysosomal biogenesis to baseline levels

Figure II-6. USF2 suppresses autophagosome formation

Figure II-7. USF2 binds promoter regions to regulate lysosomal and autophagy-related genes

Figure II-8. USF2 regulates autophagy and lysosomal genes as a transcriptional repressor

Figure II-9. USF2 modulates chromatin accessibility

Figure II-10. USF2 regulates gene expression through chromatin accessibility modulation

Figure II-11. USF2-mediated chromatin regulation via interaction with the NuRD complex

Figure II-12. USF2-NuRD complex represses gene expression by reducing H3K27Ac levels

Figure II-13. Schematic representation of the USF2-NuRD complex repression mechanism

Figure III-1. Competitive binding of USF2 and MiT/TFE family members to autophagy-related gene promoters

Figure III-2. USF2 does not affect the nuclear translocation of TFEB

Figure III-3. USF2 regulates lysosomal and autophagy gene expression through TFEB-dependent mechanisms

Figure III-4. USF2 competes with TFEB for promoter binding and regulates gene expression during nutrient starvation

Figure III-5. Phosphorylation of USF2 modulates its DNA-binding activity

Figure III-6. GSK3β-dependent Phosphorylation of USF2 regulates its DNA binding

Figure III-7. Nutrient starvation suppresses USF2 phosphorylation via inhibition of GSK3β activity

Figure III-8. USF2 promotes clearance of misfolded α1-antitrypsin aggregates

Figure III-9. Synergistic effects of TFEB overexpression and USF2 knockdown on ATZ degradation

Figure III-10. Schematics of Therapeutic Strategies for α1-Antitrypsin Deficiency through the Inhibition of USF2 and the Activation of TFEB

Figure IV-1. Schematics of the regulation of autophagy and lysosome genes by USF2 and TFEB under nutrient-rich or deficient condition

CHAPTER I
Introduction

I-1. Autophagy

1.1. General information about autophagy

Macroautophagy, commonly referred to as autophagy, is an essential and conserved cellular process critical for maintaining homeostasis. While it operates at a basal level under normal conditions, autophagy is notably upregulated in response to environmental stresses, such as nutrient starvation. This process begins with the formation of a phagophore, a membrane structure that sequesters cytoplasmic components. The phagophore then develops into a double-membraned vesicle known as an autophagosome (Klionsky and Emr 2000, Mizushima, Levine et al. 2008). The subsequent fusion of autophagosomes with lysosomes creates autolysosomes, where the degradation of intracellular components occurs. Lysosomal biogenesis and functionality are fundamental to autophagy, facilitating the breakdown and recycling of proteins, lipids, carbohydrates, and nucleic acids. Lysosomes, which contain over 60 hydrolytic enzymes and various regulatory molecules, are indispensable for cellular viability and metabolic balance (Ballabio and Bonifacino 2020). Dysregulation of lysosomal function in humans is associated with lysosomal storage diseases, where the accumulation of undigested substrates disrupts cellular and tissue function (Parenti, Andria et al. 2015, Platt, d'Azzo et al. 2018).

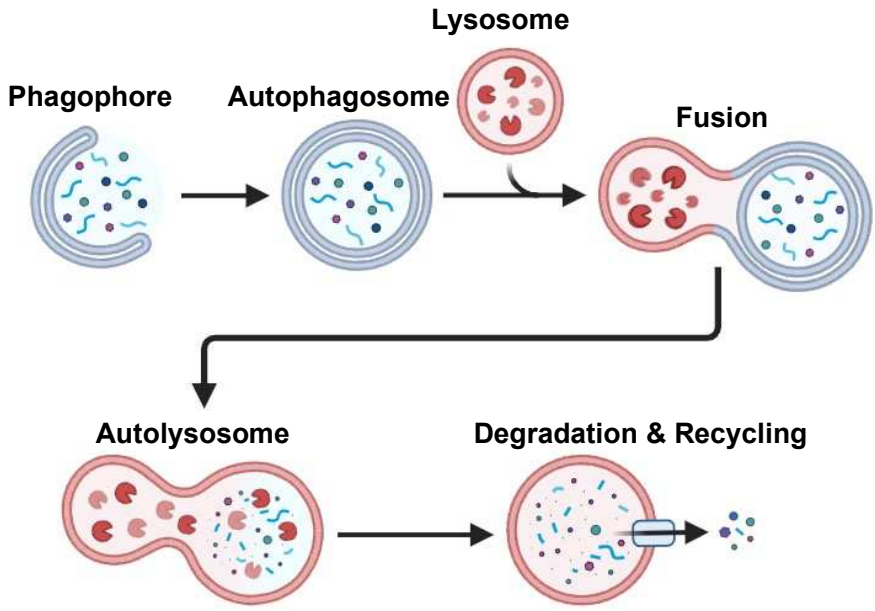

Figure I-1. Diagrammatic illustration of the autophagy process

A section of the cytoplasm is encapsulated by a forming isolation membrane, resulting in the creation of an autophagosome. The autophagosome subsequently merges with a lysosome to form an autolysosome, where its internal contents are broken down by lysosomal enzymes.

1.2. Transcriptional and epigenetic regulation of autophagy

For a long time, autophagy was primarily regarded as a process governed by cytosolic mechanisms. However, recent research has highlighted the important role of transcriptional and epigenetic regulation within the nucleus in orchestrating autophagy (Lapierre, Kumsta et al. 2015, Füllgrabe, Ghislat et al. 2016). Numerous transcription factors have been identified as key regulators of autophagy-related genes, including transcription factor EB (TFEB), forkhead box O (FOXO), p53 and cAMP response element-binding protein (CREB) (Settembre, Di Malta et al. 2011, Broz, Mello et al. 2013, Eijkelenboom and Burgering 2013, Seok, Fu et al. 2014). Additionally, post-translational modifications of histones—such as methylation, acetylation, and phosphorylation—are known to modulate the accessibility of transcription factors to chromatin. Among these, histone methylation and acetylation have been shown to play critical roles in autophagy gene regulation (Shin, Kim et al. 2016, Sakamaki, Wilkinson et al. 2017). For instance, histone H3 Lys9 di-methylation mediated by the lysine methyltransferase G9a suppresses the expression of autophagy-related genes. Conversely, CARM1-dependent histone H3 Arg17 di-methylation at the promoters of autophagy genes has been demonstrated to be essential for efficient autophagy induction. These findings underscore the importance of transcriptional and epigenetic regulation in maintaining autophagic flux and ensuring proper autophagy function. Despite these advances, the detailed molecular mechanisms underlying these regulatory processes remain insufficiently understood, necessitating further investigation.

I-2. USF2

2.1. General information about USF2

Upstream stimulatory factors (USFs), namely USF1 and USF2, are transcription factors, which bind to the 5′-CANNTG-3′ E-box core sequence (Corre and Galibert 2005). These factors regulate a variety of genes involved in cellular processes such as the cell cycle (Cogswell, Godlevski et al. 1995), immune responses (Chang, Smith et al. 1992), fatty acid synthesis (Casado, Vallet et al. 1999), insulin signaling (Wang and Sul 1995), and UV-induced pigmentation in melanocytes (Galibert, Carreira et al. 2001, Corre, Primot et al. 2004). USF1 has been linked to familial combined hyperlipidemia, a condition characterized by elevated triglycerides and/or total cholesterol that often runs in families (Pajukanta, Lilja et al. 2004). On the other hand, USF2 is involved in regulating metabolic processes (Corre, Primot et al. 2004), iron homeostasis (Nicolas, Bennoun et al. 2001), fertility (Sirito, Lin et al. 1998), and growth (Gao, Wang et al. 2003). The critical importance of USF1 and USF2 in embryonic development is demonstrated by the embryonic lethality observed in mice lacking both genes (Sirito, Lin et al. 1998). Despite these findings, there remains a lack of comprehensive understanding regarding the nuclear mechanisms that regulate the transcription of autophagy and lysosomal genes.

2.2. The structure of USF2

Upstream stimulatory factors (USF1 and USF2) belong to the basic helix-loop-helix leucine zipper (bHLH-LZ) family of transcription factors. These proteins are defined by two main structural motifs: the basic helix-loop-helix (HLH) domain and the leucine zipper (LZ) region. The HLH domain is composed of two α-helices connected by a loop, with the basic domain located within the first helix, responsible for DNA binding. This domain specifically interacts with the E-box sequence (5′-CANNTG-3′) to regulate gene transcription. The second α-helix, along with the leucine zipper, enables interaction with other bHLH-LZ transcription factors, promoting dimerization. The leucine zipper contains a heptad repeat of leucine residues, facilitating the formation of either homodimers or heterodimers. Additionally, structural analyses suggest that USF proteins can function as bivalent homotetramers, allowing them to bind to two separate E-boxes simultaneously, enhancing the coordinated regulation of multiple genes. The structural flexibility of USF proteins highlights their complexity in regulating transcription.

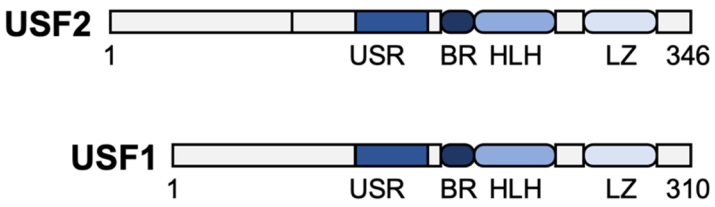

Figure I-2. Illustration of USF2 structure

USF2 is a member of the basic helix-loop-helix leucine zipper (bHLH-LZ) transcription factor family. Its structure consists of several key domains: the Basic Region (BR) responsible for DNA binding, where it interacts with the E-box motif (5′-CANNTG-3′), and the Helix-Loop-Helix (HLH) domain, composed of two α-helices connected by a loop, which facilitates dimerization with other bHLH-LZ proteins. The Leucine Zipper (LZ) region aids in stabilizing the dimer and mediating interactions with other transcription factors. Together, these domains enable USF2 to function as a homodimer or heterodimer, and it may also form a bivalent homotetramer, allowing simultaneous interaction with two distinct E-box motifs.

2.3. Phosphorylation of USF2

Phosphorylation is a critical post-translational modification regulating the function of USF2, impacting its role in transcriptional control and cellular processes. Glycogen synthase kinase-3β (GSK3β) phosphorylates USF2 at serine 155 and threonine 230, causing a conformational change that enhances its DNA-binding affinity and transcriptional activity (Horbach, Chi et al. 2014). In GSK3β-deficient cells, USF2 function is reduced, while phosphorylation-mimicking mutants restore its ability to regulate target gene expression and promote cell migration, suggesting a potential role in cancer progression.

Phosphorylation also regulates USF2 during ovulation, where it activates the prostaglandin synthase-2 (PGHS-2) promoter in granulosa cells. The luteinizing hormone (LH)-triggered cAMP/PKA pathway phosphorylates USF proteins, increasing their binding to the E-box and enhancing PGHS-2 transcription. Mutations in the phosphorylation site abolish this activity, confirming its importance (Sayasith, Lussier et al. 2005). Collectively, phosphorylation fine-tunes USF2 activity, emphasizing its essential role in transcriptional regulation in both physiological and pathological contexts.

.

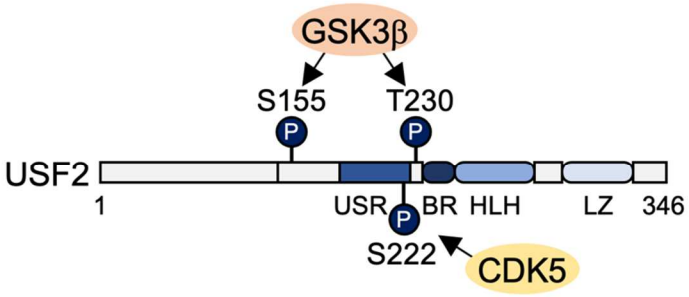

Figure I-3. Illustration of USF2 Phosphorylation

USF2 is regulated by phosphorylation at serine 155 and threonine 230, mediated by GSK3β, which enhances its DNA-binding affinity and transcriptional activity. This modification is critical for USF2 function, as its absence reduces target gene expression and cell migration. During ovulation, phosphorylation of USF proteins by the cAMP/PKA pathway increases their binding to the E-box of the PGHS-2 promoter, driving its transcription. These kinase-mediated modifications highlight phosphorylation as a key mechanism controlling USF2 activity in various biological processes.

I-3. NuRD complex

3.1. General information about NuRD complex

The Nucleosome Remodeling and Deacetylase (NuRD) complex is a key player among the four major ATP-dependent chromatin remodeling complexes. It is composed of six core subunits, each with multiple isoforms, including HDAC1/2, MTA1/2/3, RBBP4/7, GATAD2A/B, MBD2/3, and CHD3/4. MTA1/2/3 serve as scaffolding components crucial for NuRD assembly and are often overexpressed in various cancers. RBBP4 and RBBP7, while integral to NuRD, also contribute to other Class I HDAC complexes such as Sin3A and PRC2 (Le Guezennec, Vermeulen et al. 2006, Kelly and Cowley 2013, Spruijt, Luijsterburg et al. 2016). Since its discovery nearly two decades ago, understanding of NuRD has expanded significantly. Initially identified as a transcriptional repressor, it is now recognized for its more nuanced roles in regulating gene expression, including supporting gene activation. Beyond transcription, NuRD is involved in critical biological processes like DNA repair, often achieved through chromatin remodeling or post-translational modifications of transcription factors such as p53 (Allen, Wade et al. 2013, Torchy, Hamiche et al. 2015, Rother and van Attikum 2017). Recent research has revealed its diverse functional roles, offering insights into potential therapeutic applications.

3.2. Repressive mechanism of NuRD complex deacetylating H3K27Ac

The NuRD complex plays a pivotal role in chromatin remodeling and transcriptional regulation through its histone deacetylation activity, particularly targeting lysine residues such as H3K27. This activity involves the removal of acetyl groups from histone tails, notably reducing H3K27 acetylation (H3K27Ac), a mark associated with active transcription. By deacetylating H3K27, the NuRD complex promotes chromatin compaction, suppressing the accessibility of transcriptional machinery and leading to gene repression (Reynolds, Salmon-Divon et al. 2012). This dynamic regulation is critical for processes such as cell differentiation and development, where precise control of gene expression is essential. Dysregulation of NuRD-mediated H3K27 deacetylation has been implicated in pathological conditions, including cancer, underscoring its role in maintaining chromatin homeostasis and influencing transcriptional states.

I-4. α1-antitrypsin deficiency (AATD) disease

4.1. Causes of AATD

Alpha1-antitrypsin deficiency (AATD) is the most common genetic cause of liver disease in children (Sveger 1988) and is also linked to chronic liver disease and hepatocellular carcinoma in adults (Eriksson, Carlson et al. 1986, Piitulainen, Carlson et al. 2005). AAT, a serine protease inhibitor (SERPIN) family member, is synthesized in the liver and serves as the most abundant protease inhibitor in plasma. The condition exhibits considerable allelic variation, with over 70 known variants (PI types), but the majority of cases result from homozygosity for the PI*Z allele,* while non-Z variants are rare (Cox and Billingsley 1989). *The PIZ* allele encodes a mutant AAT protein, ATZ, with a lysine-to-glutamate substitution at position 342, which disrupts proper folding. This misfolded ATZ protein tends to polymerize and aggregate in the endoplasmic reticulum (ER) of hepatocytes, causing liver damage through a toxic gain-of-function mechanism. These aggregates form intrahepatocytic globules, a hallmark of the disease. Among PI*Z homozygous children, abnormal liver function is often observed in the first year of life; about 10% experience prolonged jaundice, and 2% progress to liver failure, for which liver transplantation is the only curative option (Sveger 1976, Sveger 1988).

4.2. Therapeutic approach of AATD

The intracellular accumulation of mutant alpha-1-antitrypsin Z (ATZ) triggers proteotoxic effects through mechanisms not yet fully elucidated. However, studies have revealed key cellular pathways involved in ATZ degradation and adaptation. The proteasomal and autophagic pathways are central to ATZ disposal, with the former utilizing ER-associated degradation (ERAD) to translocate misfolded ATZ from the ER to the cytoplasmic proteasome (Qu, Teckman et al. 1996, Gelling, Dawes et al. 2012). Autophagy, critical for degrading aggregated proteins, has been implicated in ATZ clearance, with its activation observed in cellular and mouse models, as well as in patients with alpha-1-antitrypsin deficiency (ATD) (Teckman and Perlmutter 2000, Kamimoto, Shoji et al. 2006). While ERAD efficiently handles lower levels of ATZ, autophagy becomes essential at higher expression levels due to the formation of insoluble aggregates (Kruse, Dear et al. 2006). Additional mechanisms, such as a sortilin-mediated Golgi-to-lysosome pathway, also contribute to ATZ degradation, suggesting a multifaceted system of disposal that may involve yet unidentified pathways (Gelling, Dawes et al. 2012). Defects in these pathways, particularly autophagy, are linked to aging and degenerative diseases, emphasizing their importance in ATD pathogenesis and potential therapeutic targeting (Gosai, Kwak et al. 2010).

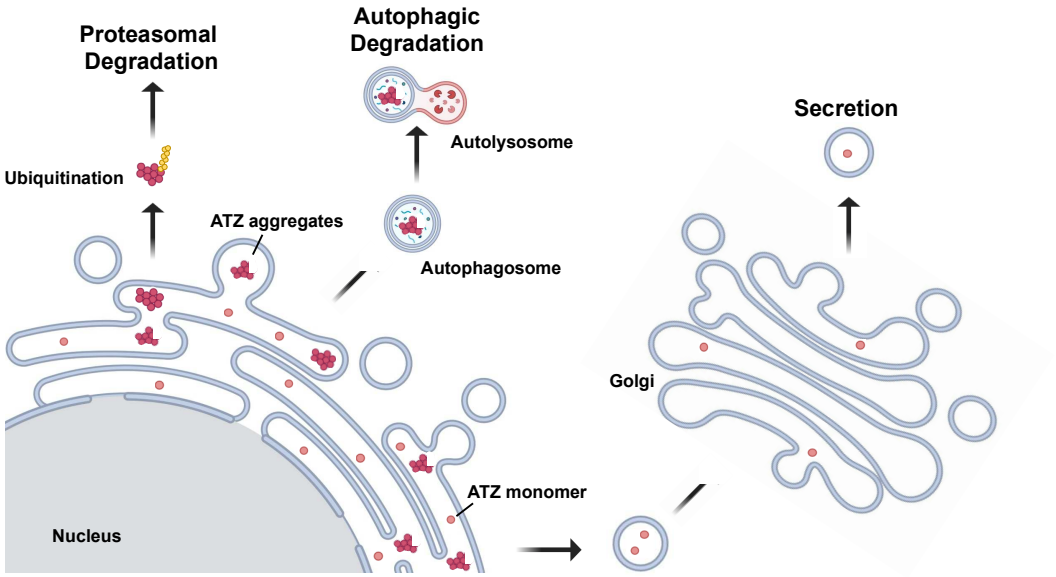

Figure I-4. Illustration of the degradation of ATZ aggregates

ATZ accumulates intracellularly, causing proteotoxic effects through mechanisms that involve key degradation pathways. The proteasomal pathway, via ER-associated degradation, and autophagy play central roles in ATZ disposal. While ERAD efficiently handles lower levels of misfolded ATZ, autophagy is critical for clearing insoluble aggregates at higher levels. Additional pathways, like the sortilin-mediated Golgi-to-lysosome route, further contribute to ATZ degradation, highlighting a complex system essential for managing proteotoxic stress and its associated diseases.

CHAPTER II

USF2 Represses Autophagy and Lysosome Biogenesis Through Epigenetic Mechanisms With the NuRD Complex

II-1. Summary

USF2 plays a critical role as a transcriptional repressor of autophagy and lysosome biogenesis by regulating lysosomal and autophagy-related genes through epigenetic mechanisms. Under nutrient-rich conditions, USF2 binds directly to gene promoters containing the CLEAR motif, where it diminishes histone H3K27Ac and restricts chromatin accessibility. This repression is mediated in part by its interaction with the NuRD complex, which includes HDAC1, collaboratively suppressing lysosomal and autophagy-related gene expression. By repressing these pathways, USF2 ensures tight regulation of lysosomal and autophagic activity, which is essential for maintaining cellular homeostasis and basal metabolism. This balance is particularly important in preventing dysregulated autophagy or lysosomal function, which can lead to cellular stress and disease. The role of USF2 in modulating these processes highlights its significance in the broader context of cellular adaptation and homeostasis. Dysregulation of this mechanism has potential implications in a variety of disorders linked to lysosomal and autophagic dysfunction, positioning USF2 as a promising therapeutic target for diseases associated with defective protein degradation or cellular stress responses.

II-2. Introduction

Autophagy is a highly conserved cellular process essential for maintaining homeostasis through the degradation and recycling of intracellular components. This process involves the formation of autophagosomes, which sequester cytoplasmic materials and subsequently fuse with lysosomes to form autolysosomes, where degradation occurs. Transcriptional and epigenetic mechanisms have emerged as crucial regulators of autophagy, with transcription factors such as TFEB, FOXO, and E2F1 playing prominent roles. Histone modifications, including methylation and acetylation, further modulate the expression of autophagy-related genes.

USF2, a member of the bHLH-LZ family, binds to E-box sequences to regulate various cellular processes, including metabolism, growth, and iron homeostasis. Despite its established roles, the precise molecular mechanisms through which USF2 influences autophagy and lysosome biogenesis remain poorly understood.

NuRD complex is a multifunctional chromatin remodeling complex involved in transcriptional repression and activation. Among its functions, the deacetylation of H3K27Ac is particularly significant in silencing gene expression by promoting chromatin compaction. Dysregulation of NuRD has been implicated in several pathological conditions, emphasizing its importance in maintaining chromatin homeostasis.

This study aims to explore the potential role of USF2 in modulating autophagy and lysosome biogenesis through epigenetic mechanisms, including its association with

chromatin modifiers such as the NuRD complex. By elucidating these regulatory pathways, I aim to deepen our understanding of the transcriptional control of autophagy and its broader implications for cellular and pathological processes.

II-3. Results

USF2 as a key transcription factor in lysosomal gene regulation identified through ChIP-seq analysis

To uncover transcription factors (TFs) associated with lysosomal gene regulation, I performed a ChIP-seq-based TF enrichment analysis focusing on lysosome-related genes. Utilizing ENCODE ChIP-seq datasets encompassing 1867 TFs, I developed a comprehensive TF binding matrix by analyzing TF interactions with promoter regions (Fig. II-1A). From this analysis, I pinpointed TFs that specifically bind to the promoters of lysosomal genes, including those differentially expressed under nutrient-starved conditions and those involved in lysosomal biogenesis (Fig. II-1B, C). Among the top candidates, USF2 emerged consistently, alongside well-characterized MiT/TFE family members such as Microphthalmia-associated transcription factor (MITF) and TFE3 (Fig. II-1D). These findings suggest that USF2 may play a regulatory role in lysosomal gene expression.

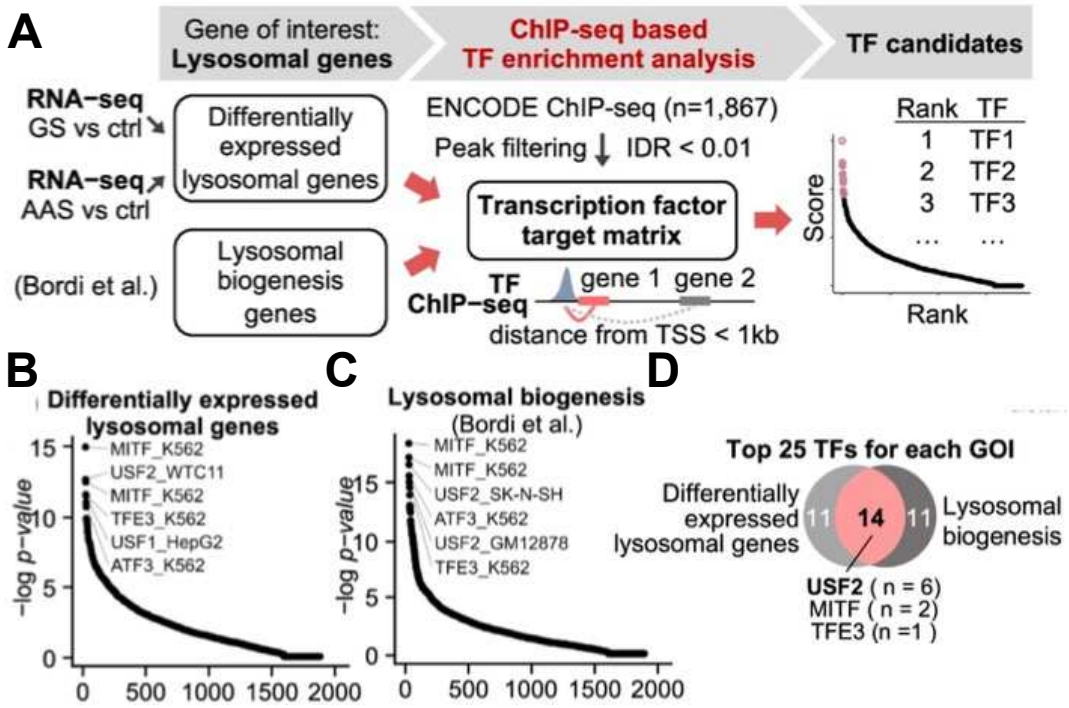

Figure II-1. USF2 as a key transcription factor in lysosomal gene regulation identified through ChIP-seq analysis

(**A**) Diagram illustrating the workflow for identifying lysosome-associated transcription factors (TFs) through a screening process, incorporating TF enrichment rankings derived from the ENCODE ChIP-seq database. (**B**) TF enrichment rank plot highlighting TFs associated with differentially expressed lysosomal genes. (**C**) TF enrichment rank plot focusing on genes linked to lysosomal biogenesis. (**D**) Venn diagram depicting the overlap of enriched TFs associated with lysosomal regulation.

USF2 knockdown enhances lysosomal biogenesis

To explore the function of USF2 in the regulation of lysosomal gene expression, I generated HepG2 cell lines with stable knockdown of USF2 using shRNA technology. The effectiveness of USF2 knockdown was confirmed by assessing the expression levels of LAMP1, a critical lysosomal membrane protein that serves as a marker for lysosomal biogenesis. Results revealed a significant upregulation of LAMP1 expression in USF2 knockdown cells compared to wild-type (WT) controls, highlighting a potential repressive role of USF2 in lysosomal gene regulation (Fig. II-2A).

To further investigate the impact of USF2 knockdown on lysosomal activity, I employed LysoSensor, a fluorescent dye that specifically labels acidic organelles such as lysosomes. Fluorescence microscopy showed markedly enhanced fluorescence signals in USF2 knockdown HepG2 cells, indicating an increase in lysosomal acidity and abundance compared to WT cells (Fig. II-2B). Moreover, a detailed analysis of lysosome morphology revealed that USF2 knockdown cells exhibited not only an increased number of lysosomes but also a noticeable enlargement in lysosomal size, suggesting enhanced lysosomal biogenesis (Fig. II-2C).

Taken together, these findings demonstrate that USF2 plays a critical role in suppressing the expression of genes related to lysosomal biogenesis. The observed increase in lysosomal number and size upon USF2 knockdown emphasizes its function as a negative regulator of lysosomal gene expression and shows its importance in maintaining lysosomal homeostasis.

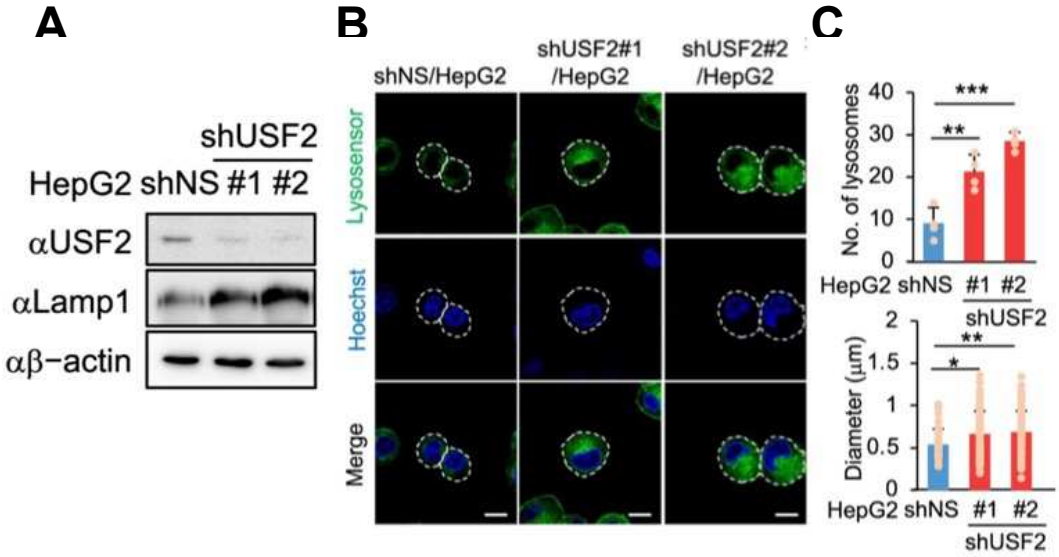

Figure II-2. USF2 knockdown enhances lysosomal biogenesis

(**A**) Immunoblot showing the expression levels of USF2 and LAMP1 in shNS (control) and shUSF2 knockdown HepG2 cell lines. (**B**) Representative confocal microscopy images displaying LysoSensor staining in shNS and shUSF2 HepG2 cells. The white outlines indicate cell boundaries. LysoSensor signals are shown in green, and Hoechst-stained nuclei are in blue. Scale bar: 20 μm. (**C**) Quantitative analysis of the lysosomal number per cell and the average diameter of lysosomes in shNS and shUSF2 HepG2 cells. Data are presented as mean values, n = 4 biologically independent samples. * $p<0.05$, ** $p<0.01$, *** $p<0.001$. Statistics by two-tailed t-test.

Generation and characterization of *Usf2*$^{-/-}$ mice revealing embryonic lethality

To investigate the *in vivo* function of USF2, I generated *Usf2*$^{-/-}$ mice by deleting exons 1–7 of the *Usf2* gene. This knockout strategy was designed to fully disrupt the expression of USF2 in these mice (Fig. II-3A). Genotyping analysis of the offspring from *Usf2* heterozygous matings at three weeks of age revealed an expected Mendelian inheritance pattern for WT and heterozygous pups. However, no homozygous *Usf2*$^{-/-}$ pups were observed, indicating that the complete loss of USF2 results in embryonic lethality. These findings suggest that USF2 is essential for embryonic development, and its absence is incompatible with postnatal survival (Fig. II-3B).

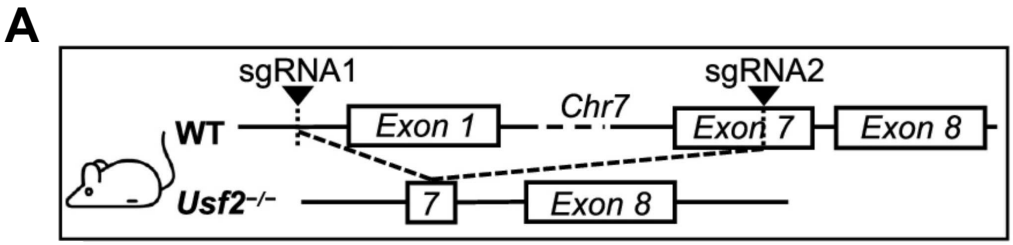

B

3−weeks mice

Usf2$^{+/-}$ x *Usf2*$^{+/-}$	Expected	Observed
+/+	16	17
+/−	32	35
−/−	16	0
Total	64	52

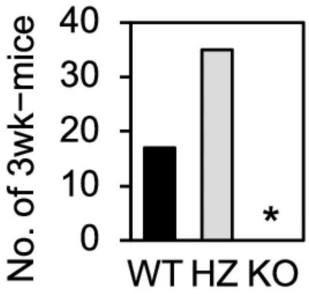

Figure II-3. Generation and characterization of *Usf2*$^{-/-}$ mice revealing embryonic lethality

(A) Schematic representation of the generation of *Usf2* whole-body knockout mice. **(B)** Genotyping results of *Usf2* heterozygous mating offspring. "Expected" refers to the theoretical number of offspring based on the Mendelian ratio, while the "Observed" values are shown in the graph on the right. The absence of homozygous *Usf2*-KO pups suggests embryonic lethality.

USF2 deficiency enhances lysosomal biogenesis and proteolytic activity

I generated WT and *Usf2*$^{-/-}$ mouse embryonic fibroblasts (MEFs) from 13.5-day-old embryos to investigate the role of USF2 in lysosomal biogenesis. Transmission electron microscopy (TEM) analysis of these MEFs revealed that *Usf2* knockout (KO) significantly increased the number of lysosomes (Fig. II-4A). These lysosomes appeared functionally mature, as indicated by their cargo content.

To validate these observations, additional experiments were conducted. Consistent with findings from USF2 knockdown in HepG2 cells, *Usf2*$^{-/-}$ MEFs exhibited elevated LAMP1 expression compared to WT MEFs (Fig. II-4B). LysoSensor staining further confirmed enhanced lysosomal biogenesis, with *Usf2*$^{-/-}$ MEFs showing stronger fluorescence and an increased number and size of lysosomes compared to their WT counterparts (Fig. II-4C, D).

The functionality of these lysosomes was assessed using DQ-BSA, a fluorescent substrate that emits fluorescence upon degradation. *Usf2*$^{-/-}$ MEFs showed approximately two-fold higher fluorescence intensity from DQ-BSA degradation products than WT MEFs, indicating increased lysosomal degradation activity (Fig. II-4E, F). Furthermore, *in vitro* cathepsin D activity assays demonstrated nearly two-fold higher proteolytic potential in *Usf2*$^{-/-}$ MEFs relative to WT MEFs (Fig. II-4G). These results establish that USF2 deficiency promotes lysosomal maturation, biogenesis, and proteolytic functionality.

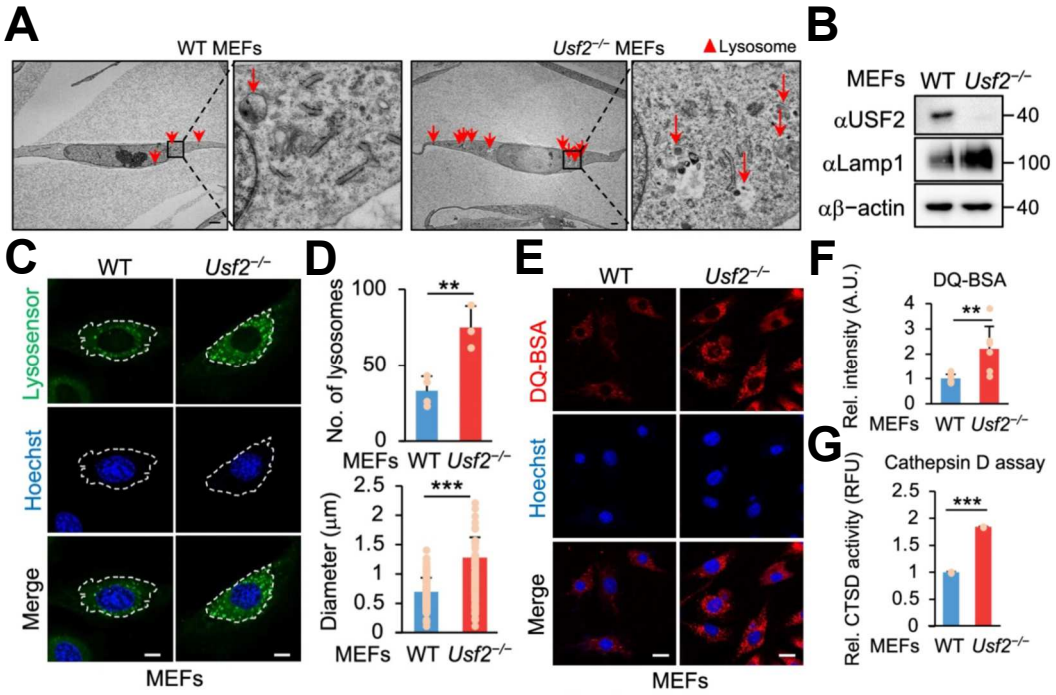

Figure II-4. USF2 deficiency enhances lysosomal biogenesis and proteolytic activity

(**A**) Representative TEM images of WT and *Usf2*$^{-/-}$ MEFs. Scale bar, 2 μm. High magnification of the boxed areas is shown on the right. Lysosomes (red arrows). (**B**) Immunoblot analysis of USF2 and Lamp1 expression in WT and *Usf2*$^{-/-}$ MEFs. (**C**) Representative confocal microscopy images showing Lysosensor staining in WT and *Usf2*$^{-/-}$ MEFs. Scale bar: 20 μm. (**D**) Quantitative analysis of lysosomal number per cell and average lysosomal diameter in WT and *Usf2*$^{-/-}$ MEFs. Data represent n = 4 biologically independent samples. (**E**) Representative confocal images of DQ-BSA staining in WT and *Usf2*$^{-/-}$ MEFs. Cells were treated with DQ-BSA to assess lysosomal degradation. DQ-BSA, red; Hoechst, blue. Scale bar: 20 μm. (**F**) Quantification of fluorescence intensity of DQ-BSA degradation products per cell in WT and *Usf2*$^{-/-}$ MEFs. Data represent n = 6 biologically independent samples. (**G**) Measurement of lysosomal cathepsin D activity in WT and *Usf2*$^{-/-}$ MEFs. Data represent n = 2 biologically independent samples. * $p<0.05$, ** $p<0.01$, *** $p<0.001$. Statistics by two-tailed t-test.

USF2 reconstitution restores lysosomal biogenesis to baseline levels

To directly examine the suppressive effect of USF2 on lysosomal biogenesis, reconstitution experiments were conducted. Reconstitution of USF2 into *Usf2*-deficient cells reversed the enhanced lysosomal biogenesis phenotype. In both *Usf2*$^{-/-}$ MEFs and USF2 knockdown HepG2 cells, USF2 reconstitution significantly reduced Lamp1 expression to levels comparable to wild-type cells (Fig. II-5A). Moreover, the number of lysosomes was also normalized to wild-type levels upon USF2 reintroduction, as shown by Lysotracker staining (Fig. II-5B, C). These findings demonstrate that USF2 acts as a transcriptional repressor of lysosomal genes, thereby functioning as a critical negative regulator of lysosomal biogenesis and function.

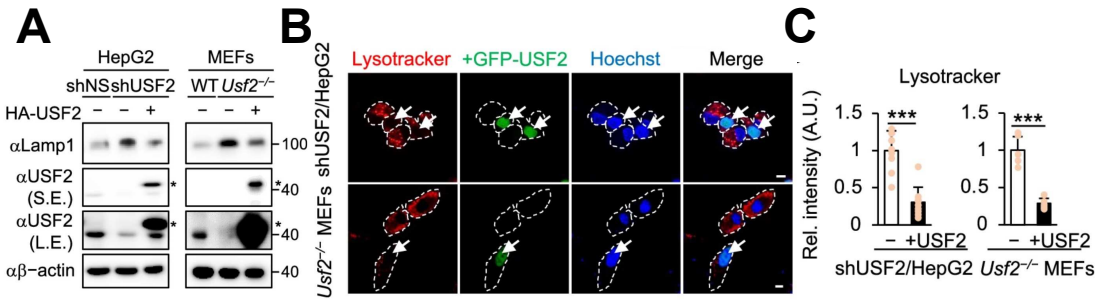

Figure II-5. USF2 reconstitution restores lysosomal biogenesis to baseline levels

(**A**) Immunoblot analysis showing LAMP1 expression in shNS, shUSF2, and GFP-USF2-reconstituted shUSF2 HepG2 cell lines (left) and in WT, *Usf2*$^{-/-}$, and GFP-USF2-reconstituted *Usf2*$^{-/-}$ MEFs (right). (**B**) Representative confocal microscopy images of Lysotracker staining in shUSF2 HepG2 cells and *Usf2*$^{-/-}$ MEFs reconstituted with GFP-USF2. Lysotracker, red; GFP, green; Hoechst, blue. Scale bar: 10 µm. (**C**) Quantitative analysis of Lysotracker intensity per cell in shUSF2 HepG2 cells (n = 9 biologically independent samples) and *Usf2*$^{-/-}$ MEFs (n = 5 biologically independent samples). Data are presented as mean ± standard error of the mean (SEM). * $p<0.05$, ** $p<0.01$, *** $p<0.001$. Statistics by two-tailed t-test.

USF2 suppresses autophagosome formation

To determine whether USF2 influences autophagic activity, I analyzed autophagic flux in *Usf2*-deficient cells using lysosomal inhibitors, including Bafilomycin A1 and Chloroquine. Immunoblot analysis showed that both inhibitors elevated the autophagosome marker LC3-II levels, even in *Usf2*$^{-/-}$ MEFs. Notably, LC3-II levels were significantly higher in *Usf2*$^{-/-}$ MEFs compared to WT cells under the same treatment conditions (Fig. II-6A, B). Additionally, an LC3-puncta staining assay revealed an increased number of LC3 puncta in *Usf2*$^{-/-}$ MEFs relative to WT cells, indicating enhanced autophagosome formation (Fig. II-6C, D). These findings demonstrate that USF2 functions as a repressor of autophagosome formation, further underscoring its role in regulating cellular degradative pathways.

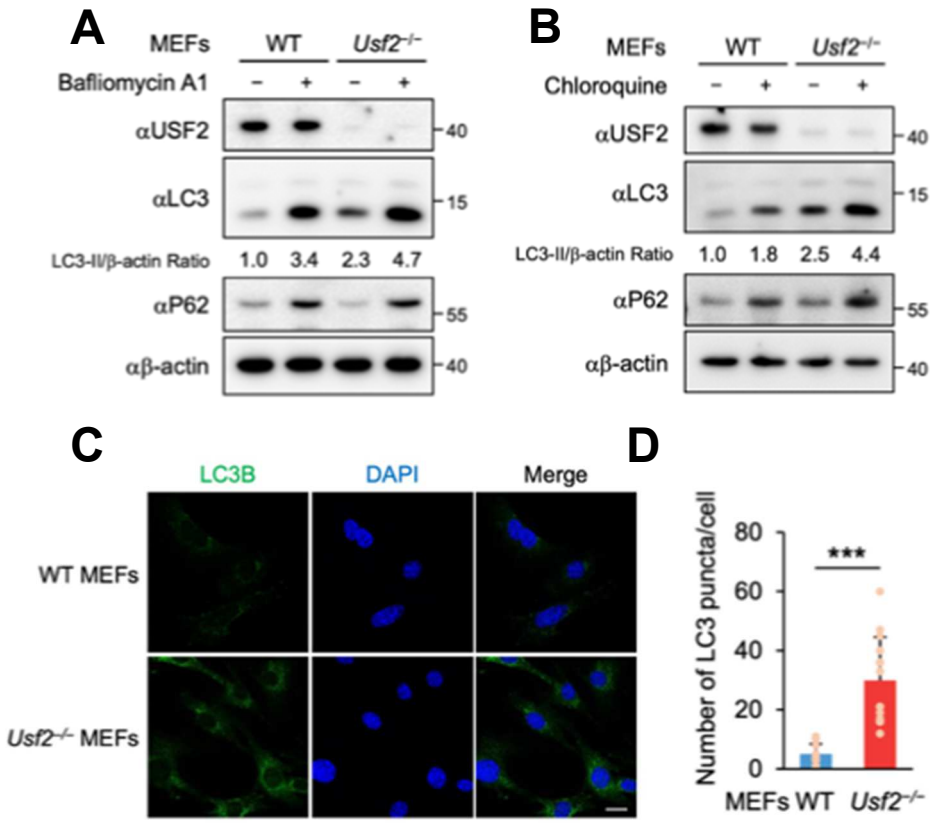

Figure II-6. USF2 suppresses autophagosome formation

(**A**-**B**) Immunoblot analyses of LC3-II levels in WT and *Usf2*$^{-/-}$ MEFs treated with lysosomal inhibitors (Bafilomycin A1 in panel **A** and Chloroquine in panel **B**). Both inhibitors induced LC3-II accumulation, with higher levels observed in *Usf2*$^{-/-}$ MEFs compared to WT cells. (**C**) Representative confocal microscopy images showing LC3 puncta in WT and *Usf2*$^{-/-}$ MEFs stained with an LC3B antibody. Images were captured under identical settings to ensure comparability. Scale bar, 10 μm. (**D**) Quantification of LC3 puncta in WT and *Usf2*$^{-/-}$ MEFs. Data represent the mean ± SEM from 14 biologically independent samples. * $p<0.05$, ** $p<0.01$, *** $p<0.001$. Statistics by two-tailed t-test.

USF2 binds promoter regions to regulate lysosomal and autophagy-related genes

To investigate the molecular mechanisms underlying USF2 function, I analyzed USF2 ChIP-seq data from the ENCODE database, focusing on histone modifications at USF2 binding sites. Examination of repetitive USF2 peaks revealed distinct patterns of histone markers (Fig. II-7A). While some sites displayed enrichment for the enhancer-associated marker H3K4me1, the majority exhibited significant enrichment for the promoter-associated marker H3K4me3, suggesting a prominent role for USF2 in transcriptional regulation at promoters. Consistently, genomic annotation showed that 65% of USF2 peaks were located within promoter regions (Fig. II-7B).

Gene ontology (GO) and Kyoto Encyclopedia of Genes and Genomes (KEGG) pathway analyses of genes with USF2-bound promoters revealed significant enrichment for terms related to autophagy and lysosomal processes, further supporting a key regulatory role for USF2 in these pathways (Fig. II-7C).

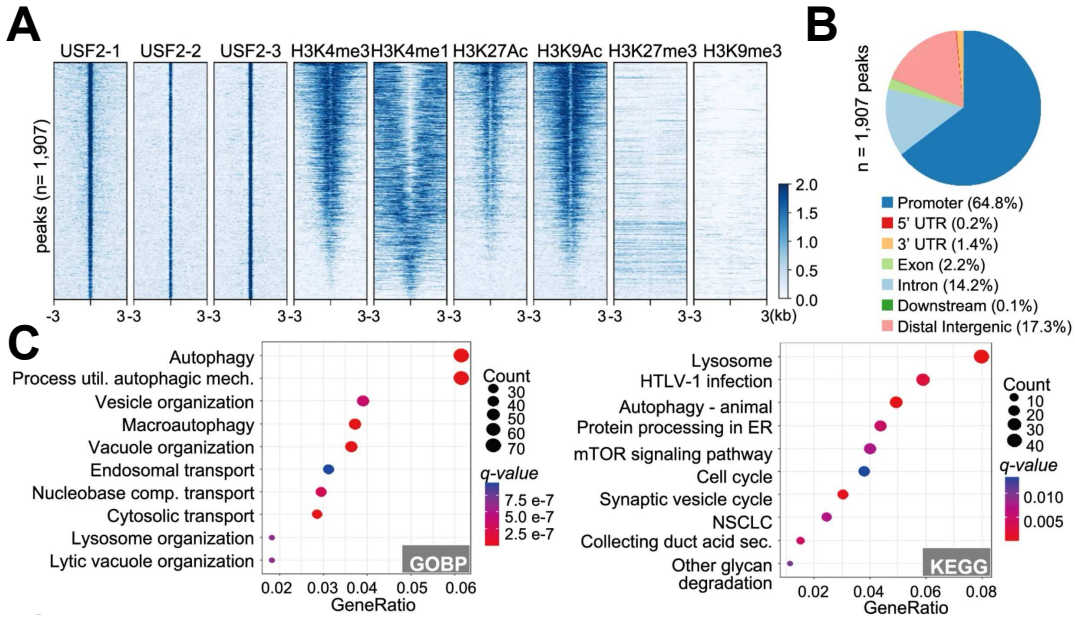

Figure II-7. USF2 binds promoter regions to regulate lysosomal and autophagy-related genes

(**A**) Heatmap showing histone marker profiles in a 6 kb window centered on USF2 binding sites. Peaks enriched for the enhancer marker H3K4me1 were observed, but most sites showed strong enrichment for the promoter marker H3K4me3. (**B**) Genomic annotation of USF2 ChIP-seq peaks. The majority of peaks (65%) were localized to promoter regions, consistent with the presence of promoter-associated histone modifications. (**C**) Gene ontology (GO) and KEGG pathway analyses of genes with USF2-bound promoters. Significant enrichment was observed for autophagy- and lysosome-related terms, highlighting USF2's functional association with these processes.

USF2 regulates autophagy and lysosomal genes as a transcriptional repressor

To uncover the mechanisms by which USF2 regulates gene expression, RNA-seq analysis was performed on WT and *Usf2*$^{-/-}$ MEFs. Differentially expressed genes (DEGs) identified in *Usf2*$^{-/-}$ MEFs were integrated with USF2 ChIP-seq data to pinpoint direct transcriptional targets of USF2. This analysis revealed 373 USF2-regulated DEGs, characterized by significant overlap between DEGs and genes bound by USF2 at their promoters (Fig. II-8A, B). Focusing on genes associated with autophagy and lysosomal pathways, a distinct pattern emerged: the majority of these genes were upregulated in *Usf2*$^{-/-}$ MEFs compared to WT MEFs (Fig. II-8C). Specifically, among the 84 autophagy- and lysosome-related genes identified, 74 were upregulated in the absence of USF2, highlighting its role as a transcriptional repressor of these pathways (Fig. II-8D). The expression of key autophagy- and lysosome-related genes such as *Ctsd, Atp6v0d1, Lamp1, Vps11*, and *Map1lc3b* was validated through qRT-PCR (Fig. II-8E) and further corroborated by immunoblotting (Fig. II-8F). These genes were consistently found to be significantly upregulated in *Usf2*$^{-/-}$ MEFs, confirming the transcriptional regulation mediated by USF2.

These findings collectively suggest that USF2 binds directly to the promoters of autophagy- and lysosome-related genes, functioning as a key transcriptional repressor. This regulation is crucial for maintaining the balance of autophagy and lysosomal biogenesis, which is disrupted in the absence of USF2.

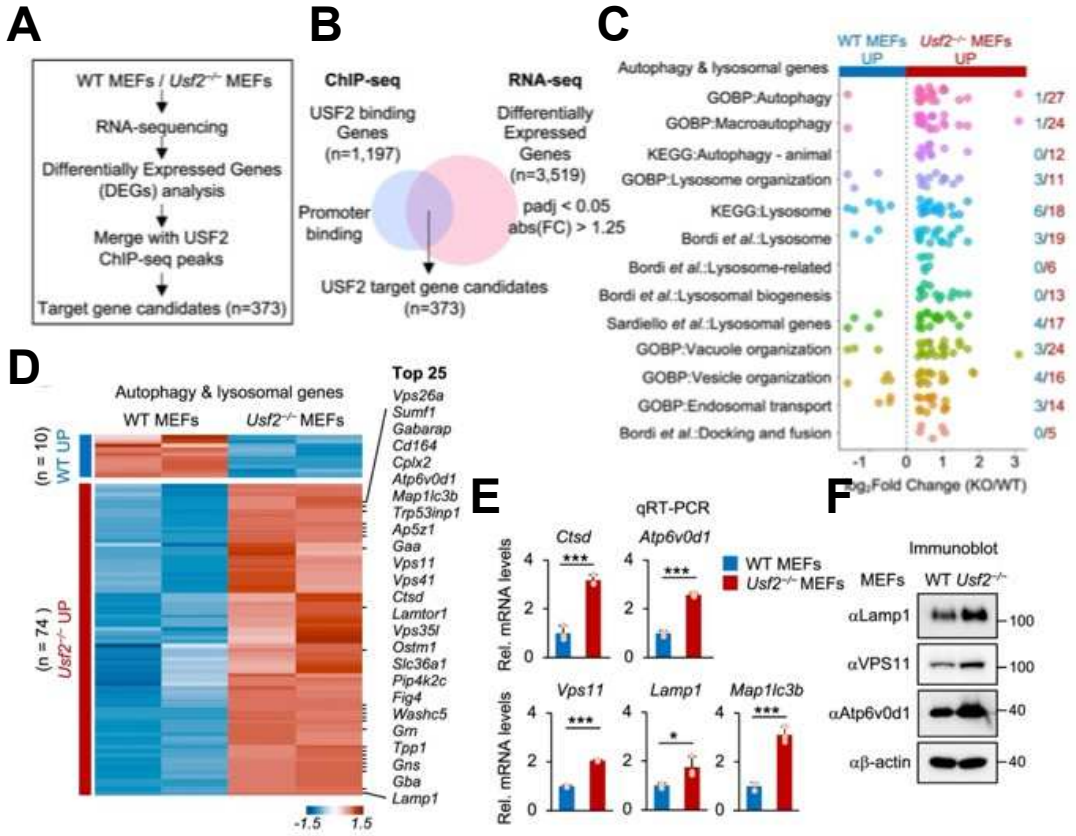

Figure II-8. USF2 regulates autophagy and lysosomal genes as a transcriptional repressor

(**A**) Schematic diagram illustrating the integrated analysis combining RNA-seq data from WT and *Usf2*$^{-/-}$ MEFs with USF2 ChIP-seq data to identify direct transcriptional targets. (**B**) Venn diagram showing 373 candidate target genes identified as USF2-bound and differentially expressed. (**C**) Distribution of fold changes in autophagy- and lysosome-related genes based on the presence or absence of USF2. Genes upregulated in WT cells are marked in blue, while those upregulated in *Usf2*$^{-/-}$ MEFs are marked in red. (**D**) Heatmap of gene expression changes in autophagy- and lysosome-related USF2 target genes. The top 25 significantly upregulated genes in *Usf2*$^{-/-}$ MEFs are listed on the right. (**E**) Quantitative RT-PCR (qRT-PCR) analysis of USF2 target genes in WT and *Usf2*$^{-/-}$ MEFs. Data represent the mean ± SEM from three technical replicates. (**F**) Immunoblot analysis confirming upregulation of lysosomal genes in *Usf2*$^{-/-}$ MEFs compared to WT MEFs. * p<0.05, ** p<0.01, *** p<0.001. Statistics by two-tailed t-test.

USF2 modulates chromatin accessibility

I examined the function of upstream stimulatory factor 2 (USF2) in repressing target gene transcription by modulating chromatin accessibility. Using ATAC-seq analysis combined with ChIP-seq data, I identified a total of 2,390 ATAC-seq peaks located within a 2-kilobase (kb) window centered around USF2 binding sites (Fig. II-9A). These peaks were found to be primarily situated within promoter regions, highlighting the potential role of USF2 in transcriptional regulation at key gene loci (Fig. II-9B).

Among the identified peaks, 456 exhibited significant differences in chromatin accessibility when comparing wild-type (WT) cells to *Usf2*$^{-/-}$ cells, suggesting that USF2 directly influences chromatin dynamics (Fig. II-9C). Interestingly, a closer analysis of these differentially opened peaks (DOPs) revealed that the majority—353 peaks—showed an increase in chromatin accessibility in *Usf2*$^{-/-}$ cells compared to WT cells. This observation strongly supports the hypothesis that USF2 functions as a repressor by restricting chromatin accessibility, thereby limiting the transcriptional activity of its target genes (Fig. II-9D).

These findings provide crucial insights into the mechanism by which USF2 mediates transcriptional repression through chromatin modulation, emphasizing its significant role in maintaining the regulatory balance of gene expression. Understanding this mechanism offers a deeper perspective on the broader implications of chromatin accessibility in cellular homeostasis and gene regulation.

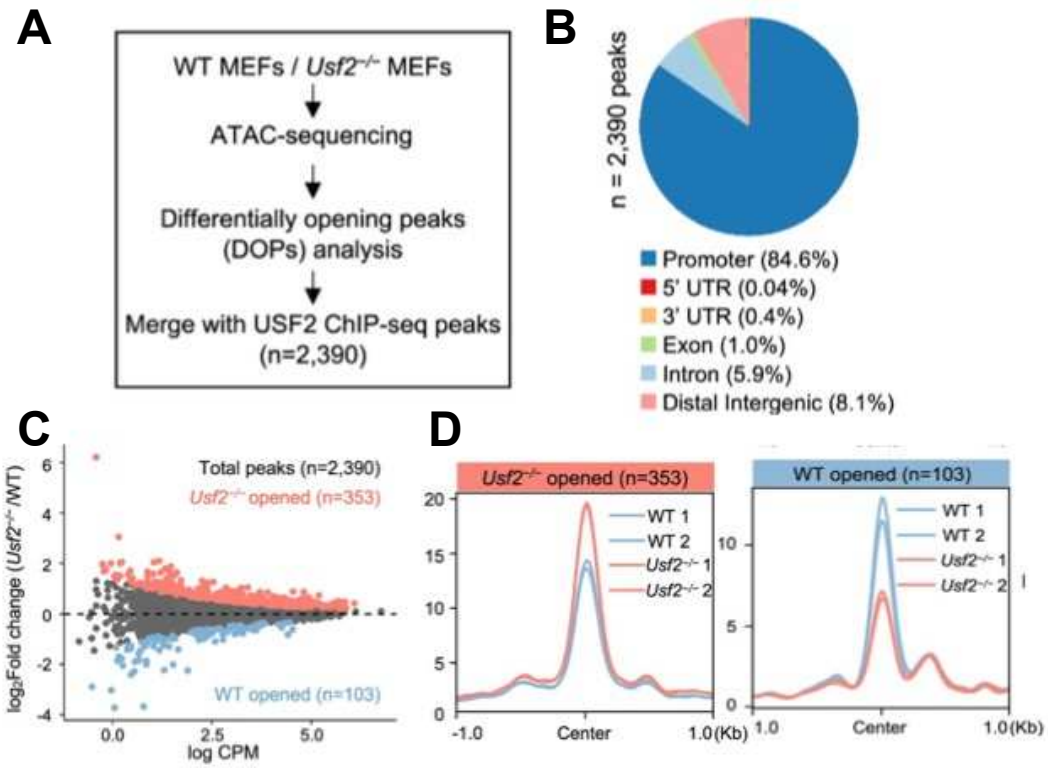

Figure II-9. USF2 modulates chromatin accessibility

(**A**) Schematic of the ATAC-seq analysis workflow, integrating USF2 ChIP-seq peaks to examine chromatin accessibility in WT and *Usf2*$^{-/-}$ MEFs. (**B**) Annotation of ATAC-seq peaks based on their genomic locations, showing a predominance of peaks within promoter regions. (**C**) Scatter plot depicting differentially opened peaks (DOPs) in WT and *Usf2*$^{-/-}$ MEFs. Peaks more accessible in *Usf2*$^{-/-}$ are shown in red, while those more accessible in WT are shown in blue. (**D**) Read density plots illustrating the accessibility of DOPs, with increased opening in *Usf2*$^{-/-}$ MEFs (left panel) and WT-specific peaks (right panel).

USF2 regulates gene expression through chromatin accessibility modulation

To elucidate the connection between USF2-mediated chromatin accessibility and gene expression, I performed an integrated multiomics analysis, combining RNA-seq, ATAC-seq, and USF2 ChIP-seq datasets. This revealed 173 differentially expressed gene (DEG)-associated differentially opened peaks (DOPs), with the majority (154) localized to promoter regions (Fig. II-10A). These promoter-specific DOPs exhibited a strong correlation between increased chromatin accessibility and changes in mRNA expression (Fig. II-10B).

Further analysis showed that 125 of the 154 promoter-associated DOPs were sites of direct USF2 binding, as identified in ChIP-seq. Notably, 114 of these regions displayed reduced mRNA expression in WT cells, highlighting USF2's role in transcriptional repression (Fig. II-10C). Gene ontology (GO) analysis revealed significant enrichment of autophagy- and lysosome-related terms among the genes with promoter-associated DOPs, emphasizing USF2's regulatory influence on these pathways (Fig. II-10D).

Focusing on autophagy and lysosomal genes, I identified 39 DEG-related DOPs, 34 of which showed increased chromatin accessibility and higher gene expression in *Usf2*$^{-/-}$ cells compared to WT cells (Fig. II-10E). Visualization of these peaks revealed the regulatory dynamics of key genes such as *Lamp1, Ctsd, Atp6v0d1,* and *Gns,* demonstrating USF2's direct binding and its repressive effect on chromatin accessibility and gene expression (Fig. II-10F). These findings establish USF2 as a critical transcriptional repressor, mediating its effects through chromatin remodeling, in genes linked to autophagy and lysosomal function.

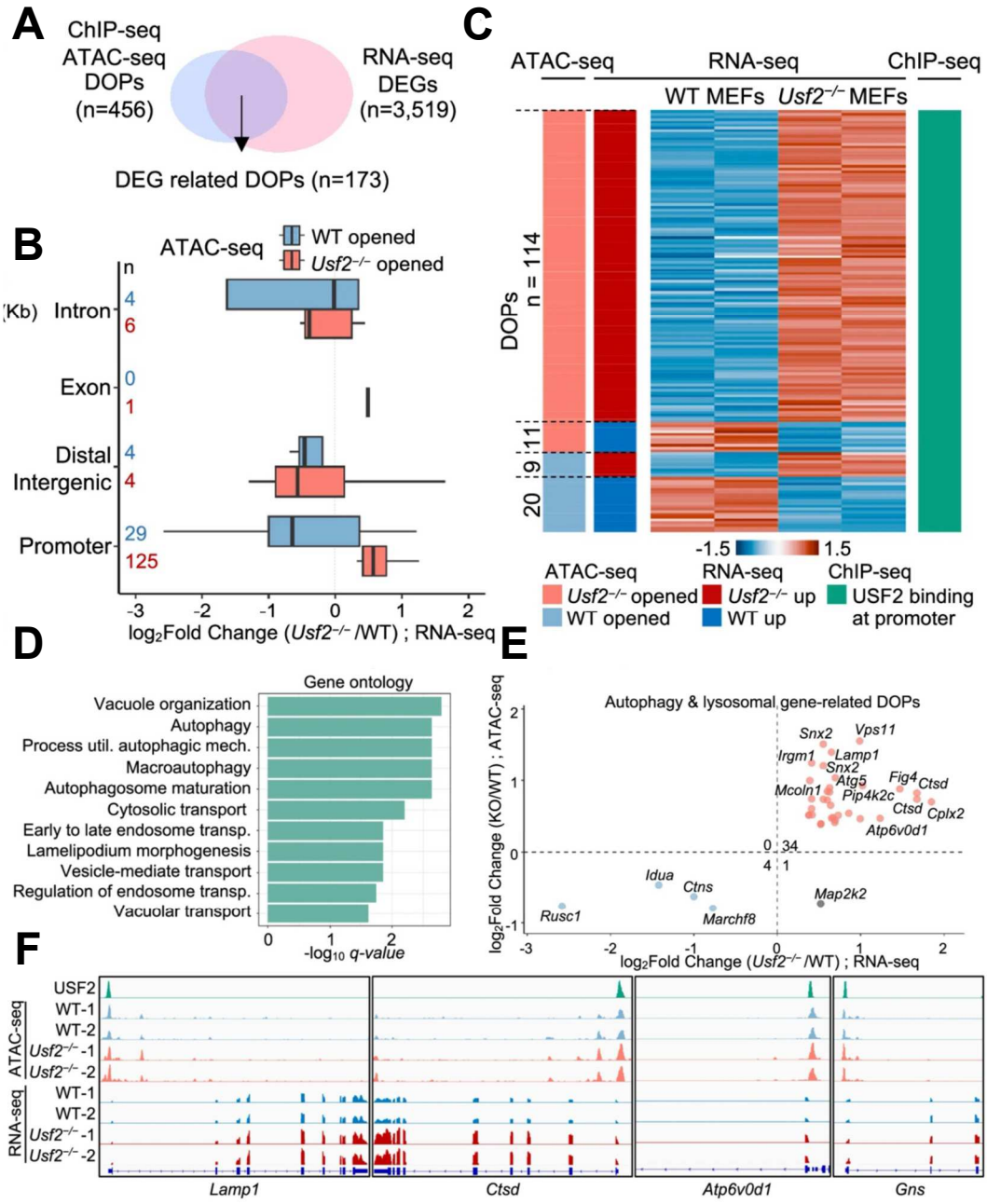
A
ChIP-seq
ATAC-seq
DOPs
(n=456)
RNA-seq
DEGs
(n=3,519)
DEG related DOPs (n=173)
B
ATAC-seq
WT opened
Usf2−/− opened
n
(Kb)
Intron
4
6
Exon
0
1
Distal
Intergenic
4
4
Promoter
29
125
-3
-2
-1
0
1
2
log2Fold Change (Usf2−/− /WT) ; RNA-seq
C
ATAC-seq
RNA-seq
ChIP-seq
WT MEFs
Usf2−/− MEFs
DOPs
n = 114
9
11
20
-1.5
1.5
ATAC-seq
Usf2−/− opened
WT opened
RNA-seq
Usf2−/− up
WT up
ChIP-seq
USF2 binding
at promoter
D
Gene ontology
Vacuole organization
Autophagy
Process util. autophagic mech.
Macroautophagy
Autophagosome maturation
Cytosolic transport
Early to late endosome transp.
Lamelipodium morphogenesis
Vesicle-mediate transport
Regulation of endosome transp.
Vacuolar transport
0
1
2
-log10 q-value
E
Autophagy & lysosomal gene-related DOPs
log2Fold Change (KO/WT) ; ATAC-seq
Snx2
Vps11
Irgm1
Lamp1
Snx2
Atg5
Fig4
Ctsd
Mcoln1
Pip4k2c
Ctsd
Cplx2
Atp6v0d1
0
34
4
1
Idua
Ctns
Map2k2
Rusc1
Marchf8
2
1
0
-1
-3
-2
-1
0
1
2
log2Fold Change (Usf2−/− /WT) ; RNA-seq
F
ATAC-seq
RNA-seq
USF2
WT-1
WT-2
Usf2−/− -1
Usf2−/− -2
WT-1
WT-2
Usf2−/− -1
Usf2−/− -2
Lamp1
Ctsd
Atp6v0d1
Gns

Figure II-10. USF2 regulates gene expression through chromatin accessibility modulation

(**A**) Venn diagram depicting 173 DEG-associated DOPs, derived by integrating RNA-seq, ATAC-seq, and ChIP-seq data. (**B**) Box plot illustrating the expression changes in genes nearest to DEG-related DOPs, highlighting promoter-specific changes. The numbers represent the count of DOPs in each category. (**C**) Heatmap showing the expression of genes closest to DEG-associated DOPs, with the top genes exhibiting USF2-dependent repression highlighted. (**D**) Gene ontology analysis of genes with DOPs in their promoters, enriched for autophagy and lysosomal pathways. (**E**) Correlation between chromatin accessibility and gene expression changes in DOPs associated with autophagy and lysosomal genes. (**F**) Visualization of USF2 ChIP-seq peaks, ATAC-seq signals, and RNA-seq coverage for selected USF2 target genes (*Lamp1, Ctsd, Atp6v0d1, Gns*), demonstrating the regulatory impact of USF2 on chromatin accessibility and transcription.

USF2-mediated chromatin regulation via interaction with the NuRD complex

To further understand the molecular mechanisms underlying USF2-mediated repression of lysosomal and autophagy gene expression, I hypothesized that USF2 recruit corepressor complexes to achieve its transcriptional effects. Using biochemical purification followed by LC-MS/MS analysis, I identified potential binding partners of USF2 (Fig. II-11A). Among the candidates, the NuRD complex, including histone deacetylases (HDAC) 1 and 2, exhibited the highest −log10(FDR) scores, suggesting a strong association with USF2 (Fig. II-11B, C).

ChIP-seq data from the ENCODE database revealed significant enrichment of NuRD complex components (HDAC1, HDAC2, CHD4, GATAD2A, GATAD2B, and MTA1) at USF2-binding sites, supporting co-recruitment of these proteins to genomic regions targeted by USF2 (Fig. II-11D). Functional validation through co-immunoprecipitation assays demonstrated direct interaction between USF2 and key NuRD components, particularly HDAC1, HDAC2, and MTA1 (Fig. II-11E). These findings suggest that USF2 collaborates with the NuRD complex to modulate chromatin accessibility, likely through the deacetylation of histone H3K27Ac, leading to transcriptional repression of target genes.

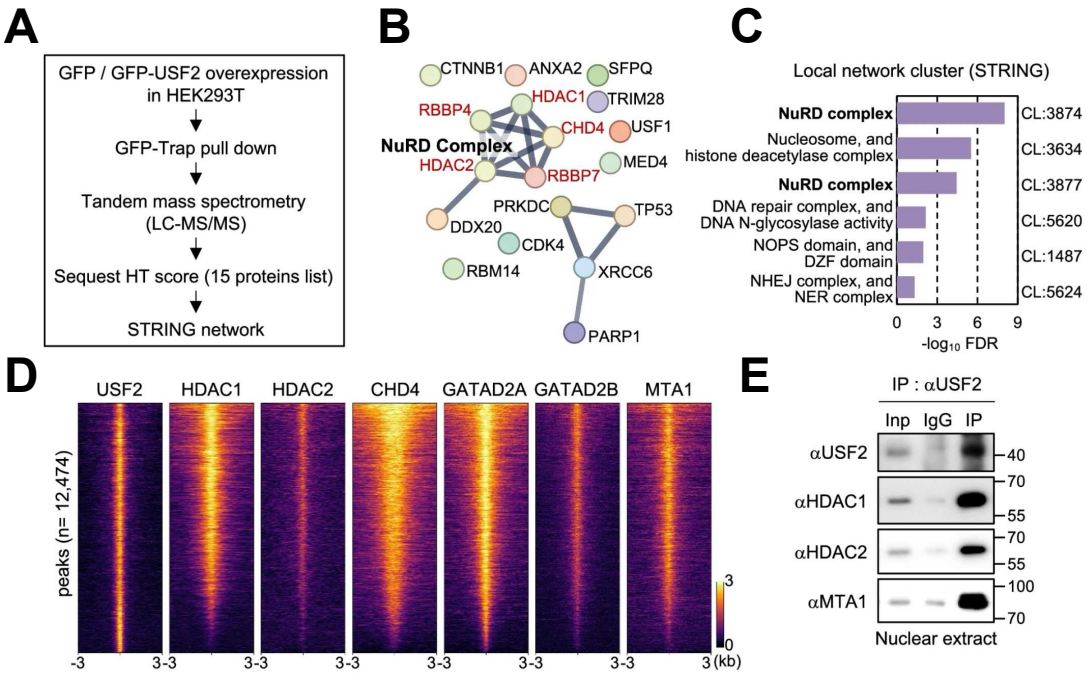

Figure II-11. USF2-mediated chromatin regulation via interaction with the NuRD complex

(**A**) Experimental flowchart for identifying USF2-binding proteins via biochemical purification followed by LC-MS/MS analysis. (**B**) Visualization of USF2-binding partner networks, analyzed through the STRING database. (**C**) Local network cluster analysis of USF2-binding partners, highlighting the NuRD complex as a key interaction cluster. (**D**) Heatmap showing the enrichment of NuRD complex components at USF2-binding sites. Each row represents a 6 kb window centered on a USF2-binding site. (**E**) Co-immunoprecipitation assay results demonstrating interaction between USF2 and NuRD complex subunits. Immunoprecipitation was performed by pulling down USF2, followed by immunoblotting with anti-HDAC1, anti-HDAC2, and anti-MTA1 antibodies. Representative images and corresponding statistics were derived from three independent experimental replicates.

USF2-NuRD complex represses gene expression by reducing H3K27Ac levels

To understand how USF2 exerts its transcriptional repression, I analyzed the histone acetylation landscape in WT and *Usf2*$^{-/-}$ MEFs using ChIP-seq. The results showed significantly higher H3K27Ac peaks in *Usf2*$^{-/-}$ MEFs, particularly at the promoter regions of *Lamp1, Atp6v0d1,* and *Gns,* compared to WT MEFs, suggesting a reduction in deacetylation activity in the absence of USF2 (Fig. II-12A, B).

Further validation using ChIP assays revealed co-recruitment of USF2 and HDAC1 to promoters of autophagy and lysosomal genes. This interaction resulted in decreased H3K27Ac levels at these loci in WT cells, confirming that the NuRD complex mediates USF2's role in transcriptional repression by histone deacetylation (Fig. II-12C). These findings highlight the critical role of USF2 and the NuRD complex in controlling chromatin accessibility and transcriptional regulation.

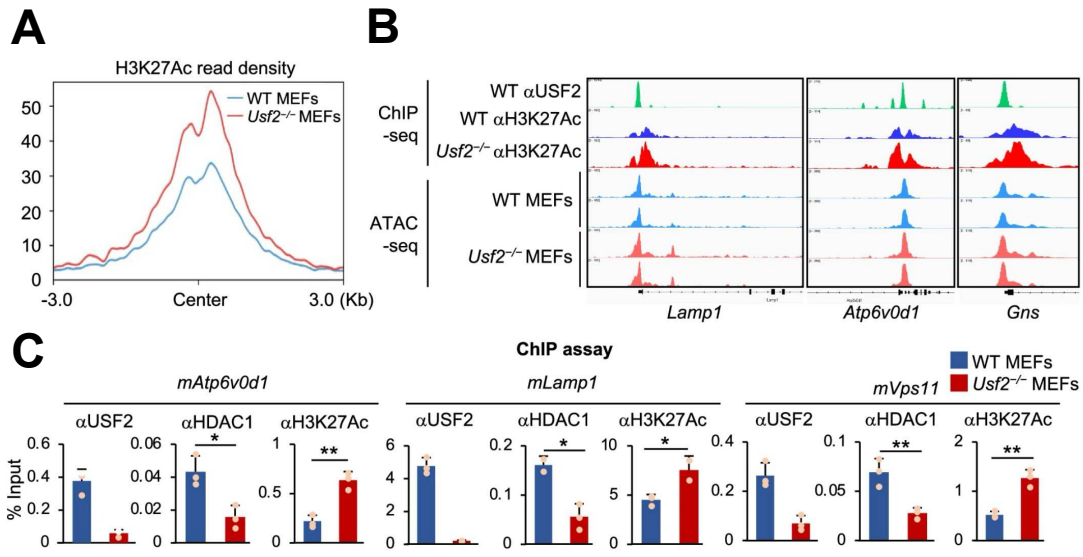

Figure II-12. USF2-NuRD complex represses gene expression by reducing H3K27Ac levels

(**A**) Read density plots showing ChIP-seq peaks of H3K27Ac in WT and *Usf2*$^{-/-}$ MEFs, with higher peaks observed in *Usf2*$^{-/-}$ MEFs. (**B**) Visualization of USF2 and H3K27Ac ChIP-seq peaks, along with ATAC-seq signals, in the promoter regions of target genes, including *Lamp1, Atp6v0d1,* and *Gns.* (**C**) ChIP assays demonstrating co-recruitment of USF2 and HDAC1 to the promoter regions of autophagy and lysosomal genes. H3K27Ac levels were quantified in WT and *Usf2*$^{-/-}$ MEFs using three technical replicates. * $p<0.05$, ** $p<0.01$, *** $p<0.001$. Statistics by two-tailed t-test.

II-4. Discussion

In this study, I identified USF2 as a key transcriptional repressor that modulates chromatin accessibility and gene expression of autophagy and lysosomal genes through its interaction with the NuRD complex. The absence of USF2 leads to increased chromatin accessibility and higher expression of autophagy-related genes, emphasizing its crucial role in maintaining homeostatic transcriptional control under normal conditions. Through integrated RNA-seq, ATAC-seq, and ChIP-seq analyses, I demonstrated that USF2 directly binds to the promoter regions of target genes, where it recruits the NuRD complex to mediate histone deacetylation (H3K27Ac) and suppress transcriptional activation.

Interestingly, my findings revealed that USF2 binds to chromatin at promoter regions to modulate accessibility and associates with the NuRD complex to repress transcription via histone modifications. This repressive mechanism is particularly evident in autophagy and lysosomal genes, where the loss of USF2 results in increased chromatin accessibility and gene expression. The co-recruitment of USF2 and NuRD complex components, including HDAC1 and HDAC2, was confirmed through both biochemical purification followed by LC-MS/MS and ChIP assays. These results establish USF2 as a critical factor linking chromatin remodeling to transcriptional regulation in response to physiological conditions.

Through genome-wide analysis, I identified 173 differentially expressed genes (DEGs) associated with differentially open chromatin regions (DOPs), with most of these DOPs

located at promoter regions. Promoter-associated DOPs showed a strong correlation between increased chromatin accessibility and higher mRNA expression in the absence of USF2, reinforcing the role of USF2 as a chromatin remodeler. GO analysis further revealed that USF2 targets were enriched in autophagy and lysosomal processes, providing a mechanistic link between USF2-mediated chromatin remodeling and cellular homeostasis.

Additionally, ChIP-seq analysis revealed higher levels of H3K27Ac in *Usf2*$^{-/-}$ cells compared to WT, particularly at the promoters of key autophagy and lysosomal genes, such as *Lamp1*, *Atp6v0d1*, and *Gns*. The absence of USF2 disrupted the NuRD-mediated deacetylation process, further supporting its role in transcriptional repression. These results underscore the importance of USF2 in orchestrating the chromatin landscape and transcriptional activity of autophagy-related genes.

Taken together, my findings demonstrate that USF2 functions as a central regulator of autophagy and lysosomal gene expression by recruiting the NuRD complex to promoter regions, thereby reducing chromatin accessibility and repressing transcription. The increased chromatin accessibility and gene expression observed in *Usf2*$^{-/-}$ cells suggest that USF2-NuRD complex activity is important for maintaining proper transcriptional control of these genes. Future studies should investigate the broader physiological implications of USF2-mediated chromatin remodeling and its potential role in autophagy-related diseases, as well as explore the molecular mechanisms that govern USF2-NuRD complex recruitment and activity at target loci.

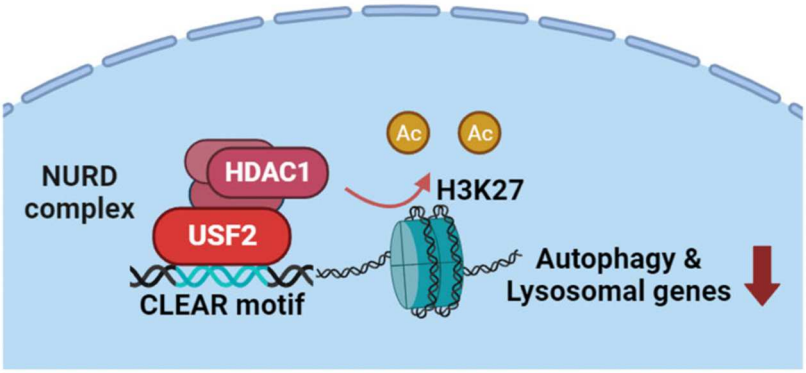

Figure II-13. Schematic representation of the USF2-NuRD complex repression mechanism

The USF2-NuRD complex represses chromatin accessibility and gene expression by deacetylating H3K27Ac, thereby limiting transcriptional activation of lysosomal and autophagy-related genes.

II-5. Materials and Methods

Reagents

The following commercially available antibodies were used; anti-USF2 (ab125184, Abcam), anti-TFEB (ab2636, Abcam), anti-HDAC1 (C15410325-50, Diagenode), anti-CTSD (sc-377299, Santa Cruz), anti-ATP6V0D1 (ab202897, Abcam), anti-VPS11 (ab125083, Abcam), anti-Lamp1 (ab24170, Abcam), anti-LC3 (ab48394, ab51520, Abcam), anti-SQSTM1/p62 (ab101266, Abcam), anti-H3K27Ac (ab4729, Abcam), anti-GSK3β (sc-81462, Santa Cruz), anti-Phospho-GSK3β (Ser9) (9323, Cell Signaling Technology) and anti-β-actin (A1978, Sigma-Aldrich). The following chemicals were used in this study; Bafilomycin A1 (11038, Sigma), Lysosensor (L7535, Thermo Fisher Scientific), Lysotracker Green (L7526, Thermo Fisher Scientific), Lysotracker Red (L7528, Thermo Fisher Scientific) and DQ Red BSA (D12051, Thermo Fisher Scientific).

Cell culture and generation of shRNA knockdown cells

WT HepG2, shUSF2 HepG2, WT MEFs, *Usf2*$^{-/-}$ MEFs, and HeLa cells were cultured at 37 °C in Dulbecco's modified Eagle's medium (DMEM) containing 10 % fetal bovine serum (FBS) and antibiotics in a humidified incubator with 5 % CO_2. All cell lines were tested for mycoplasma contamination. For glucose starvation, cells were washed with DPBS and incubated with glucose-free DMEM supplemented with 10 % dialyzed FBS. Transfection was performed using Lipofectamine 3000 (L3000075, Invitrogen) according

to the manufacturer's protocol. To generate USF2 knockdown cells, lentiviral shRNA constructs were first transfected along with viral packaging plasmids (psPAX2 and pMD2.G) into HEK293T cells. Three days after transfection, viral supernatant was filtered through 0.45 μ m filter and infected into targeting cells. Infected cells were then selected with 5 μg/ml puromycin. The targeting sequences of shRNAs are as follows.

hUSF2-1; 5′-TCCAGACTGTAACGCAGACAA-3′,

hUSF2-2; 5′-CGGCGACCACAACATCCAGTA-3′.

Generation of *Usf2* $^{-/-}$ mice and MEFs

Usf2 mutant mice were generated by introducing the gRNA/Cas9 RNP solution into fertilized eggs from the mating of B6D2F1 mice, as previously described (Noda, Sakurai et al. 2019). The gRNA sequences used were 5′-GAGCCGCTTGCGCTGATCAC-3′ and 5′-GCTCTTCTTCTCTCATCTCG-3′. By mating the resulting *Usf2*$^{+/-}$ mice (founder generation) with wild-type mice, I established *Usf2* mutant mice with a 2112 bp deletion in the *Usf2* gene. Frozen spermatozoa from B6D2-*Usf2*, RBRC#11002, and CARD#2909 will be available through RIKEN BRC (http://en.brc.riken.jp/index.shtml) and CARD R-BASE (https://cardmice.com/rbase/). All animal experiments were conducted under protocols approved by the Institutional Animal Care and Use Committee (IACUC) of Seoul National University (SNU-200901-5-3).

WT and *Usf2*$^{-/-}$ MEFs were generated by crossing two *Usf2*$^{+/-}$ mice. The pregnant female *Usf2*$^{+/-}$mice were euthanized at 13.5 days post-coitum (dpc). The embryos were

dissected by removing their heads, limbs, gonads, tail, and other visceral masses. The embryos were then chopped and digested with 0.25 % trypsin/ethylenediaminetetraacetic acid (EDTA). The enzymatic activity was neutralized by adding DMEM with 10 % FBS and antibiotics. The tissues were pipetted up and down to obtain a single-cell suspension. The cells were cultured in 100 mm culture dishes until 70–80 % confluency and sub-cultured at a ratio of 1:4. MEFs were used at different passages (P1–10).

Preparation of whole-cell lysates

All cells were briefly rinsed with cold PBS before harvesting. For whole-cell lysates, the cells were resuspended in RIPA buffer (150 mM NaCl, 1 % Triton X-100, 1 % sodium deoxycholate, 0.1 % SDS, 50 mM Tris-HCl [pH 7.5], and 2 mM EDTA) supplemented with protease inhibitors and sonicated using a Branson Sonifier 450 at output 3 and a duty cycle of 30 for five pulses. For the cytosolic and nuclear fractions, cells were lysed in harvest buffer (10 mM HEPES [pH 7.9], 50 mM NaCl, 0.5 M sucrose, 0.1 mM EDTA, 0.5 % Triton X-100, DTT, PMSF, and protease inhibitors), incubated on ice for 5 min, and centrifuged at 120 × *g* for 10 min at 4 °C. The supernatant (cytosolic fraction) was transferred into a separate tube. The nuclear pellet was rinsed twice with 500 µl of buffer A (10 mM HEPES [pH 7.9], 10 mM KCl, 0.1 mM EDTA, and 0.1 mM EGTA) and centrifuged at 120 × *g* for 10 min at 4 °C. The supernatant was discarded, and the pellet (nuclear fraction) was resuspended in RIPA buffer and sonicated. All lysates were quantified using the Bradford method and analyzed by SDS–PAGE.

Immunofluorescence analysis

Immunocytochemistry was performed as described previously (Shin, Kim et al. 2016). Cells grown on coverslips at a density of 3×10^4 cells/well in a 12-well plate were washed with PBS and fixed with 2 % formaldehyde in PBS for 10 min at room temperature. Fixed cells were permeabilized with 0.5 % Triton X-100 in PBS (PBS-T) and blocking step was performed with 3 % bovine serum albumin (BSA) in PBS-T for 1 h. Cells were incubated with antibodies overnight at 4 °C, followed by incubation with fluorescently labeled secondary antibodies for 1 h (Invitrogen), and mounted and visualized under a confocal microscope (Zeiss, LSM700). For autophagy studies, MEFs were cultured in complete medium or glucose-starved medium for 24 h.

Lysotracker and Lysosensor assays

Cells were stained with 500 nM Lysotracker Green (L7526, Thermo Fisher Scientific), Lysotracker Red (L7528, Thermo Fisher Scientific) or Lysosensor (L7535, Thermo Fisher Scientific) for 4 h (25 °C, 5 % CO_2). After washing with the probe-free medium, the samples were observed using a confocal microscope (Zeiss, LSM 700).

DQ red BSA assay

Proteolytic activity of lysosomes in the cells was measured using DQ Red BSA (D12051, Thermo Fisher Scientific). The cells were plated at a density of 10,000 cells/well in 60 mm confocal dishes. The medium was replaced with DMEM high glucose with 20 μg/ml DQ

red BSA and incubated for 4 h (25 °C, 5 % CO_2). The fluorescent signal was measured using a confocal microscope (LSM 700, Zeiss).

Quantitative RT-PCR

All Total RNA was extracted using Trizol (15596026, Invitrogen), and reverse transcription was performed from 1 μg of total RNA using an SRK-1000 SuPrimeScript cDNA Synthesis Kit (Genet Bio, Daejeon, Republic of Korea). The abundance of mRNAs was detected using an ABI prism 7500 system or BioRad CFX384 with SYBR TOPreal qPCR 2× PreMix (RT500, Enzynomics). The amount of mRNA was calculated using the ΔΔCt method, and *Hprt* was used as a control. All reactions were performed in triplicates. The following mouse primers were used in this study;

Ctsd; forward (fwd) 5′- TAAGACCACGGAGCCAGTGTCA-3′,

reverse (rev) 5′- CCACAGGTTAGAGGAGCCAGTA-3′;

Atp6v0d1; forward (fwd) 5′- GCATCTCAGAGCAGGACCTTGA-3′,

reverse (rev) 5′- GGATAGGACACATGGCATCAGC-3′;

Vps11; forward (fwd) 5′- ATCGGCAGTCTCTGGCTAATGC-3′,

reverse (rev) 5′- GGACCTTGATGGCTGTCTCTAC-3′;

Lamp1; forward (fwd) 5′- CCAGGCTTTCAAGGTGGACAGT-3′,

reverse (rev) 5′- GGTAGGCAATGAGGACGATGAG-3′;

Map1lc3b; forward (fwd) 5′- GTCCTGGACAAGACCAAGTTCC-3′,

reverse (rev) 5′- CCATTCACCAGGAGGAAGAAGG-3′;

ChIP and qRT–PCR analyzes

ChIP assays were performed as previously described (Shin, Kim et al. 2016). Cells were cross-linked in 1 % formaldehyde for 10 min and washed with ice-cold PBS three times. After glycine quenching for 5 min, the cells were collected and lysed in a buffer containing 50 mM Tris–HCl (pH 8.1), 10 mM EDTA, and 1 % SDS, supplemented with a complete protease inhibitor cocktail (11873580001, Roche). After DNA fragmentation through sonication, chromatin extracts containing DNA fragments with an average of 250 bp were then diluted ten times with dilution buffer containing 1 % Triton X-100, 2 mM EDTA, 150 mM NaCl, and 20 mM Tris–HCl (pH 8.1) with complete protease inhibitor cocktail and subjected to immunoprecipitations overnight at 4 °C. Immunocomplexes were captured by incubating 40 μl of protein A/G Sepharose for 1.5 h at 4 °C. Beads were washed with TSE I buffer (0.1 % SDS, 1 % Triton X-100, 2 mM EDTA, 20 mM Tris–HCl (pH 8.1), and 150 mM NaCl), TSE II buffer (0.1 % SDS, 1 % Triton X-100, 2 mM EDTA, 20 mM Tris–HCl (pH 8.1), and 500 mM NaCl), buffer III (0.25 M LiCl, 1 % NP-40, 1 % deoxycholate, 10 mM Tris–HCl (pH 8.1), and 1 mM EDTA), three times TE buffer (10 mM Tris–HCl (pH 8.0) and 1 mM EDTA) and eluted in elution buffer (1 % SDS and 0.1 M $NaHCO_3$). The supernatant was incubated overnight at 65 °C to reverse crosslink and then digested with RNase A for 1 h at 37 °C and proteinase K for 2 h at 55 °C. ChIP and input DNA were then purified and analyzed for qRT–PCR analysis or used for constructing sequencing libraries.

The following primers were used;

Atp6v0d1; forward (fwd) 5′- CAACTAGACTCCCCGGATCA-3′,

reverse (rev) 5′- GTCGGGCACTCCAGAGTAA-3′;

Lamp1; forward (fwd) 5′- GTGGGGAGAGGGCAAGATA-3′,

reverse (rev) 5′- CGCCAGCTTACTCCTCACTT−3′;

Vps11; forward (fwd) 5′- TCCTTCACCAGCTCCTTCTC-3′,

reverse (rev) 5′- GAGCAGCAAGCCTTTTGTG-3′;

Ctsd; forward (fwd) 5′- CGGCTTATAGGCAGGATGAC-3′,

reverse (rev) 5′- GTGCGTAGGCCTGGAGTAGG-3′;

RNA-seq analysis

RNA-seq libraries were prepared using the TruSeq Stranded mRNA LT Sample Prep Kit (Illumina) according to the manufacturer's instructions. RNAseq libraries were paired-end sequenced on an Illumina HiSeq 4000 (Macrogen). RNA-seq data were mapped using STAR (v2.7.10b) against the mouse genome (GRCm38). Read counts were generated by featureCounts (v2.0.3). The differential gene expression analysis was performed using Bioconductor package DESeq2 (v1.38.3). A clustering heatmap was drawn using a z-score that is scaled across samples for each gene. Functional enrichment analysis of GOBPs and KEGG pathways was performed using a clusterProfiler.

ChIP-seq analysis

ChIP-seq libraries were prepared for sequencing using the TruSeq DNA Sample Prep Kit, according to the manufacturer's instructions. ChIPseq libraries were paired-end sequenced on an Illumina HiSeq 4000 (Macrogen). ChIP-seq reads were aligned to the mouse reference genome (GRCm38) using Bowtie2 (v2.5.1). Peaks were called using Macs2 (v2.2.7.1). BigWig files were generated using bamCoverage (v3.5.1). USF2 upon glucose starvation was compared against control input. I used anti-USF2 and anti-H3K27Ac antibodies for ChIP-seq.

ATAC-seq analysis

ATAC-seq libraries were prepared for sequencing using Illumina Tagment DNA TDE1 Enzyme and Buffer Kits (#20034197, Illumina) and paired-end sequencing was performed by Illumina HiSeq 4000 (Macrogen). ATAC-seq reads were aligned to the mouse reference genome (GRCm38) using Bowtie2 (v2.5.1). Peaks were called using Macs2 (v2.2.7.1). BigWig files were generated using bamCoverage (v3.5.1).

LC–MS/MS analysis

Transfected HEK293T cells were lysed with EBC200 buffer (50 mM Tris-HCl [pH 8.0], 200 mM NaCl, 0.5% NP-40, and protease inhibitor) and followed by centrifugation. Supernatant was incubated with GFP-Trap at 4 °C for 1 hr. The beads were washed with EBC200 buffer twice. The remaining supernatant is removed. The elutes were obtained with 100 ml acidic elution buffer (200 mM glycine [pH 2.5]) and neutralized by 10 µl neutralization buffer (1 M Tris [pH 10.4]). A Thermo Scientific Quadrupole-Orbitrap

instrument (Thermo Scientific, USA) equipped with Dionex U 3000 RSLCnano HPLC system was used. Mass spectrometric analyzes were performed using a Thermo Scientific Orbitrap Exploris 240 mass spectrometer. Fractions were reconstituted in solvent A (Water/Acetonitrile (98:2 v/v), 0.1 % Formic acid) and then injected into LC-nano ESI-MS/MS system. Samples were first trapped on a Acclaim PepMap 100 trap column (100 μm × 2 cm, nanoViper C18, 5 μm, 100 Å, Thermo Scientific, part number 164564) and washed for 6 min with solvent A (water/ACN (98:2 v/v), 0.1 % Formic acid at a flow rate of 4 μL/min, and then separated on a PepMap RSLC C18 column (75 μm × 15 cm, nanoViper C18, 3 μm, 100 Å, Thermo Scientific, part number ES900) at a flow rate of 300 nL/min. The LC gradient was run at 2% to 8% solvent B over 10 min, then from 8% to 30% over 55 min, followed by 90% solvent B (100% ACN and 0.1% Formic acid) for 4 min, and finally 2% solvent B for 20 min. Xcaliber software version 4.4 was used to collect MS data. The Orbitrap analyzer scanned precursor ions with a mass range of 350–1800 m/z with 60,000 resolution at m/z 200. Mass data are acquired automatically using proteome discoverer 2.5 (Thermo Scientific, USA). $n = 1$ for technical replicates.

Statistical analysis

Experiments were performed independently at least three times. Random images were chosen for Lysotracker and DQ red BSA intensity counting. Lysotracker and DQ red BSA staining intensity was measured using ImageJ. *P* values were calculated using two-tailed *t*-tests. For animal studies, sample size was determined empirically based on previous studies to ensure appropriate statistical power. Mice were randomly chosen for fasting. No animals

were excluded from statistical analysis, and the investigators were not blinded to the study. Values are expressed as mean ± SD. Significance was analyzed using a two-tailed, unpaired *t*-test. Statistical significance was set at $p < 0.05$.

CHAPTER III

USF2 Competes With TFEB to Regulate Autophagy and Lysosome Genes and application to α1-Antitrypsin Deficiency

III-1. Summary

Although autophagy occurs in the cytoplasm, increasing evidence suggests that transcriptional and epigenetic regulation in the nucleus are crucial for its regulation. Among the key nuclear regulators, the MiT/TFE family of transcription factors, including TFEB, plays a pivotal role in activating autophagy and lysosomal genes via the CLEAR motif. However, these processes are subject to intricate regulation by other transcription factors.

In this study, I identified USF2 as a novel repressor that antagonizes TFEB activity through competitive binding to lysosomal gene promoters. USF2 binds to E-box motifs overlapping with the CLEAR motif, thereby repressing the transcription of autophagy and lysosomal genes. Phosphorylation of USF2 at S155 by GSK3β enhances its DNA-binding ability, which further strengthens its antagonism of TFEB. Under nutrient-starved conditions, the reduced activity of GSK3β decreases USF2 phosphorylation, allowing TFEB to access promoters and activate autophagic responses.

Perturbation experiments demonstrated that the phosphorylation state of USF2 determines its functional activity. Phospho-deficient mutants (S155A) fail to repress lysosomal gene expression, while phospho-mimetic mutants (S155E) retain repression even under starvation conditions, blocking TFEB recruitment. GSK3β inhibitors like LiCl mimic nutrient starvation by reducing USF2 phosphorylation and DNA binding.

Additionally, this study explored the role of USF2 in the clearance of misfolded protein aggregates, particularly in the context of α1-antitrypsin deficiency. In cells with impaired USF2 function, enhanced lysosomal biogenesis and more efficient clearance of ATZ aggregates were observed. These results suggest that USF2 represses lysosomal activity, and inhibiting USF2 could improve the degradation of protein aggregates associated with α1-antitrypsin deficiency. Together, these findings establish USF2 as a competitive regulator of TFEB-mediated transcription and highlight its role in autophagy regulation and protein aggregate clearance in diseases like α1-antitrypsin deficiency.

III-2. Introduction

The regulation of autophagy extends beyond the cytoplasm, involving complex transcriptional and epigenetic control within the nucleus. One of the key transcription factors involved in autophagy regulation is transcription factor EB (TFEB), which acts as a master regulator of both autophagy and lysosomal biogenesis. TFEB regulates the expression of numerous genes involved in these processes, responding to environmental signals such as nutrient availability and cellular stress. This transcriptional program is critical for maintaining lysosomal function and metabolic homeostasis, highlighting the important role of TFEB in adapting to fluctuating cellular conditions (Settembre, Di Malta et al. 2011). However, while much is known about TFEB's activation, the identification of transcriptional repressors that balance autophagy-related gene expression to maintain homeostasis remains an understudied area. The discovery of such repressors would be crucial in understanding how cells fine-tune autophagic flux, ensuring cellular stability under varying conditions.

Moreover, post-translational modifications of transcription factors, particularly phosphorylation, play a significant role in regulating autophagy. USF2 is a transcription factor whose activity is tightly controlled by phosphorylation. GSK3β phosphorylates USF2 at specific sites, such as serine 155 and threonine 230, leading to conformational changes that enhance its DNA-binding affinity and transcriptional activity. In the absence of GSK3β or when phosphorylation is disrupted, USF2’s ability to regulate its target genes is compromised, impairing key transcriptional programs involved in cellular processes.

Phosphorylation of USF2 also has physiological implications, such as during ovulation, where LH-triggered signaling activates USF proteins to regulate key genes like the *PGHS-2* promoter in granulosa cells (Sayasith, Lussier et al. 2005, Horbach, Chi et al. 2014).

In the context of diseases like α1-antitrypsin deficiency, autophagy plays a critical role in the degradation of misfolded proteins. AATD is the most common genetic cause of liver disease in children and is also linked to chronic liver disease and hepatocellular carcinoma in adults (Eriksson, Carlson et al. 1986, Sveger 1988). The condition is caused by mutations in the AAT gene, with the most common mutation being the PIZ allele, which leads to the production of the misfolded ATZ protein. This misfolded protein aggregates in the liver, leading to hepatotoxicity. While the proteasomal pathway is responsible for degrading lower levels of misfolded ATZ, autophagy becomes essential for the clearance of larger, insoluble aggregates (Teckman and Perlmutter 2000, Kamimoto, Shoji et al. 2006). Dysregulation of autophagy contributes to the pathogenesis of AATD, underscoring its importance in cellular protein quality control and as a potential therapeutic target (Gosai, Kwak et al. 2010).

This study aims to investigate the competitive relationship between USF2 and TFEB in the regulation of autophagy and cellular homeostasis. I will explore how USF2 phosphorylation influences this dynamic, focusing on the mechanisms by which phosphorylation modulates USF2's transcriptional activity and its interaction with TFEB, shedding light on their coordinated role in transcriptional regulation under physiological and pathological conditions, including AATD.

III-3. Results

Competitive binding of USF2 and MiT/TFE family members to autophagy-related gene promoters

In silico motif analysis of USF2-binding regions identified a predominant 5′-GTCACGTG-3′ sequence, which corresponds to the E-box motif (Fig. III-1A). Notably, TFE3 and MITF, known regulators of autophagy and lysosome-related genes, showed high enrichment at these sites, suggesting their potential to bind to the E-box motif (Fig. III-1A). However, TFEB was not detected in this analysis due to limited ENCODE data. All members of the MiT/TFE family, including TFE3 and MITF, are known to interact with the CLEAR motif (Fig. III-1B). Examination of human ChIP-seq data confirmed that TFE3 and MITF bind to the same genomic regions as USF2 (Fig. III-1B, C), with peak visualization revealing their binding to USF2 target genes such as *Lamp1*, *Vps11*, *Atp6v0d1*, and *Gaa* (Fig. III-1D). ChEA transcription factor enrichment analysis, utilizing genes upregulated in *Usf2* knockout models (Fig. III-1E), indicated TFEB and MITF as the most enriched transcription factors for these genes (Fig. III-1F). Perturbation analysis further suggested that genes repressed by USF2 were most similar to those upregulated upon TFEB overexpression (Fig. III-1G). These findings led to the hypothesis that USF2 and the MiT/TFE family members antagonistically regulate gene expression by competing for the same binding motifs.

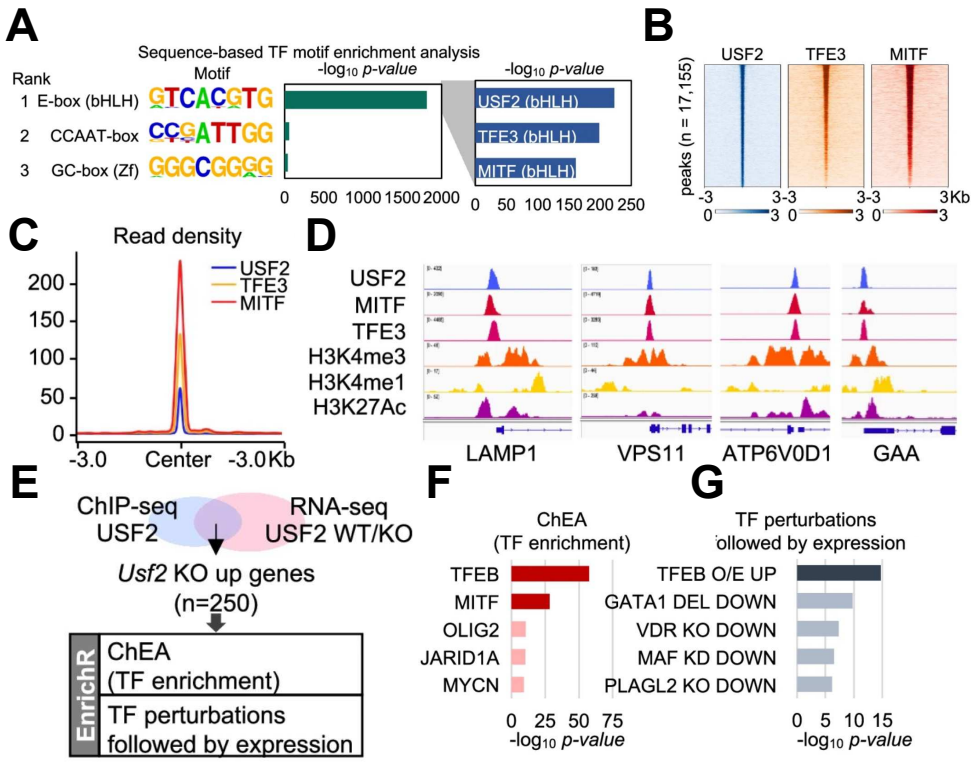

Figure III-1. Competitive binding of USF2 and MiT/TFE family members to autophagy-related gene promoters

(**A**) a. In silico motif analysis of USF2 ChIP-seq data, identifying the E-box motif (5′-GTCACGTG-3′) at USF2 binding sites. (**B**) Heatmap illustrating the enrichment of TFE3 and MITF at USF2 binding sites, with each row representing a 6 kb window centered on a USF2 binding site. (**C**) Read density plots for ChIP-seq peaks of USF2, TFE3, and MITF, showing their binding at common genomic regions. (**D**) Visualization of ChIP-seq peaks for USF2, MITF, TFE3, and histone modification markers (H3K4me3, H3K4me1, H3K27Ac) at USF2 target genes. (**E**) EnrichR gene set analysis of genes repressed by USF2. (**F**) ChEA transcription factor enrichment analysis of genes upregulated in *Usf2* knockout models, highlighting the enrichment of TFEB and MITF. (**G**) TF perturbation analysis using genes upregulated in *Usf2* knockout models, revealing similarities to genes upregulated by TFEB overexpression.

USF2 does not affect the nuclear translocation of TFEB

To investigate the role of USF2 in regulating TFEB localization, I performed immunoblotting analysis, cell fractionation, and immunocytochemistry using an anti-TFEB antibody. These analyses revealed that glucose starvation (GS) did not induce any observable difference in the translocation of TFEB between WT and *Usf2*$^{-/-}$ MEFs (Fig. III-2A, B, C). Additionally, I assessed the recruitment of TFEB to the promoters of target genes in *Usf2*$^{-/-}$ cells during glucose starvation. ChIP assays showed that glucose starvation indeed increased TFEB recruitment to the promoter regions in *Usf2*$^{-/-}$ cells (Fig. III-2D). These findings suggest that USF2 does not impact the nuclear translocation of TFEB.

Although TFEB predominantly resides in the cytoplasm under steady-state conditions, its localization is dynamically regulated by the balance between nuclear export and import processes. Thus, even under steady-state conditions, TFEB is able to activate the expression of its target genes, which can be inhibited by USF2. I further confirmed the presence of TFEB in the nucleus even at steady-state conditions.

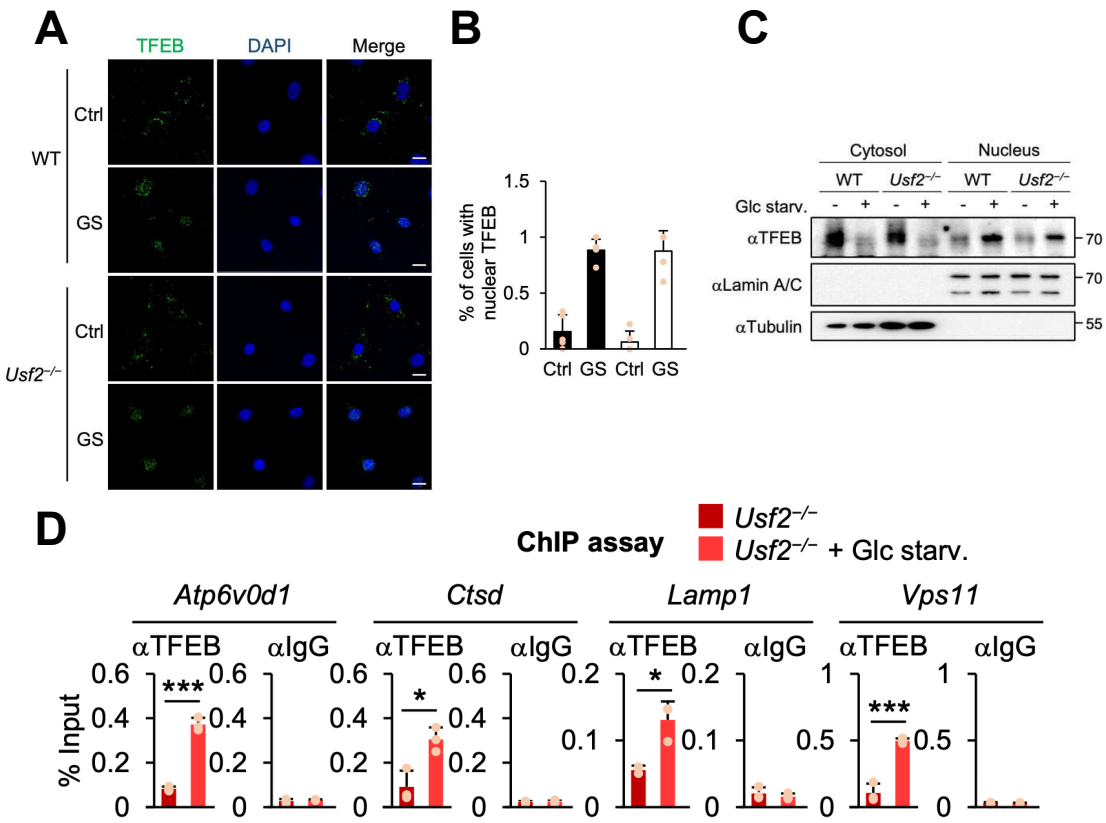

Figure III-2. USF2 does not affect the nuclear translocation of TFEB

(**A**) Representative confocal images of TFEB staining under normal and glucose starvation (GS) conditions in WT and *Usf2*$^{-/-}$ MEFs. Anti-TFEB antibody staining is shown in green, and DAPI (nuclear stain) is shown in blue. Scale bar = 20 µm. (**B**) Quantification of the percentage of cells with nuclear TFEB in WT and *Usf2*$^{-/-}$ MEFs, based on immunocytochemical analysis. Data are derived from n = 6 biologically independent samples. (**C**) Immunoblot analysis of TFEB localization in WT and *Usf2*$^{-/-}$ MEFs, using cell fractionation to separate cytoplasmic and nuclear fractions. (**D**) ChIP assay analysis of lysosomal gene promoters under normal and GS conditions in *Usf2*$^{-/-}$ MEFs. n = 3 technical replicates. * $p<0.05$, ** $p<0.01$, *** $p<0.001$. Statistics by two-tailed t-test.

USF2 regulates lysosomal and autophagy gene expression through TFEB-dependent mechanisms

I investigated the role of USF2 in regulating the recruitment of TFEB to the promoters of target genes under steady-state conditions. ChIP assays demonstrated enhanced recruitment of TFEB to target gene promoters in *Usf2* knockout cells compared to WT cells (Fig. III-3A). Further analysis showed that the knockdown of TFEB by siRNA in *Usf2* knockout or knockdown cells resulted in reduced expression of autophagy and lysosomal genes (Fig. III-3B, C). Additionally, the increased levels of histone modification H3K27Ac in *Usf2* knockout cells were reversed following TFEB knockdown (Fig. III-3D). I also considered the potential compensatory roles of TFEB homologs, such as TFE3 and MITF, which are known to regulate lysosomal biogenesis and autophagy in a cooperative and partially overlapping manner. Consequently, the partial reduction in the effect of TFEB knockdown may be attributed to these homologs. Overall, these results suggest that USF2 modulates autophagy and lysosomal gene expression in a TFEB-dependent manner under steady-state conditions.

To further explore the interaction between USF2 and glucose starvation, I used ChIP-seq to examine the occupancy of USF2 at target gene promoters. Upon glucose starvation, I observed a reduction in USF2 ChIP peaks across all target genes, suggesting that USF2 remains bound to its target gene promoters under normal conditions but dissociates under

glucose starvation. This finding contrasts with TFEB's behavior, which increases recruitment to target gene promoters under glucose starvation (Fig. III-3E). ChIP assays confirmed that USF2 recruitment to the promoters of genes such as *Atp6v0d1*, *Lamp1*, and *Ctsd* was reduced under both glucose starvation and amino acid starvation (AAS) (Fig. III-3F, G).

.

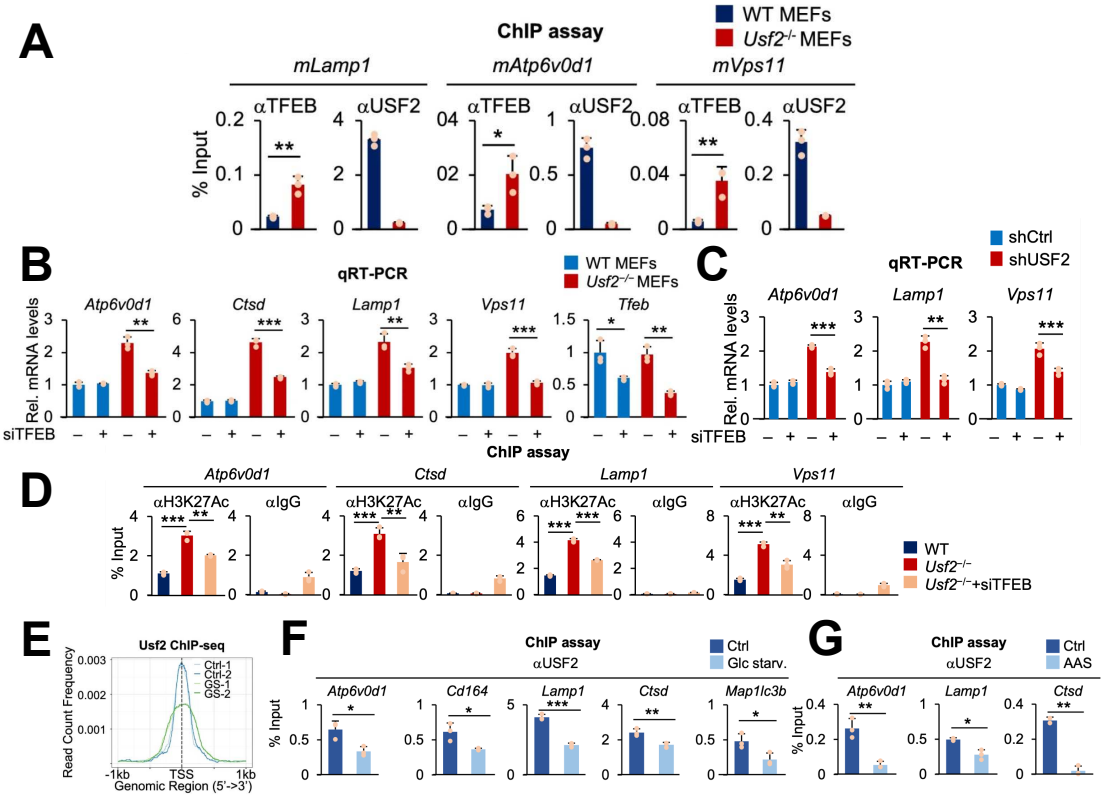

Figure III-3. USF2 regulates lysosomal and autophagy gene expression through TFEB-dependent mechanisms

(**A**) ChIP assays on USF2-dependent promoters in WT and *Usf2*$^{-/-}$ MEFs using anti-TFEB and anti-USF2 antibodies. n = 3 technical replicates. (**B**) qRT-PCR assay of USF2 target genes in WT and *Usf2*$^{-/-}$ MEFs with or without TFEB knockdown. n = 3 technical replicates. (**C**) qRT-PCR assay of USF2 target genes under siNS and siTFEB treatment in shCtrl and shUSF2 HepG2 cells. n = 3 technical replicates. (**D**) Individual ChIP assay on lysosomal gene promoters in WT, *Usf2*$^{-/-}$ MEFs and *Usf2*$^{-/-}$ MEFs under siTFEB treatment. n = 3 technical replicates. (**E**) Normalized USF2 ChIP-seq peaks under normal and GS conditions. (**F**) Individual ChIP assay on USF2-dependent promoters under normal and GS conditions. n = 3 technical replicates. (**G**) Individual ChIP assay on USF2-dependent promoters under normal and AAS conditions. n = 3 technical replicates. * p<0.05, ** p<0.01, *** p<0.001. Statistics by two-tailed t-test.

USF2 competes with TFEB for promoter binding and regulates gene expression during nutrient starvation

I further examined whether TFEB and USF2 bind competitively to the same promoter regions by using the Lamp1 promoter-luciferase reporter containing the CLEAR motif. TFEB alone upregulated luciferase activity, but co-transfection with USF2 inhibited this activation (Fig. III-4A). Notably, overexpression of USF2 WT repressed TFEB-induced luciferase activity, while the USF2 DNA-binding domain mutant failed to repress it (Fig. III-4A). These results suggest that USF2's DNA-binding ability is critical for competing with TFEB in transcriptional repression. ChIP assays showed that glucose starvation reduced USF2 recruitment to the Lamp1 promoter but increased TFEB binding to this region (Fig. III-4B). To explore the role of USF2 during nuclear co-localization with TFEB, I performed RNA-seq under glucose and amino acid starvation. Despite TFEB translocating to the nucleus under these conditions, USF2-mediated gene repression persisted. In contrast, in the absence of USF2, target gene expression was hyperactivated during both glucose and amino acid starvation (Fig. III-4C, D).

I also examined USF2 recruitment and H3K27Ac levels at USF2 target gene promoters in TFEB-deficient cells. In the context of glucose starvation, TFEB depletion led to an increase in USF2 recruitment to lysosomal gene promoters and a decrease in their H3K27Ac levels (Fig. III-4E).

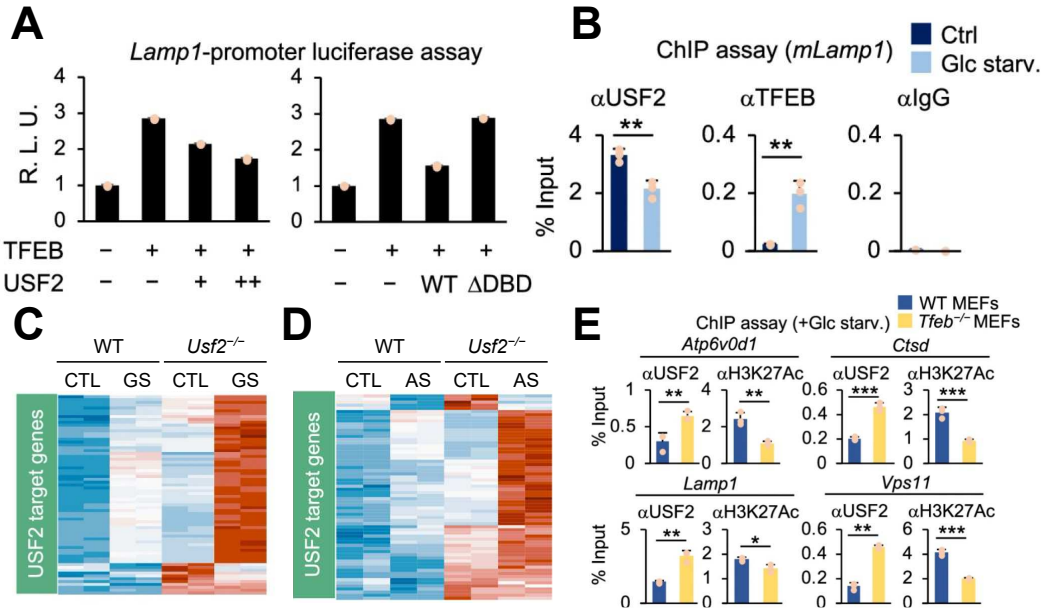

Figure III-4. USF2 competes with TFEB for promoter binding and regulates gene expression during nutrient starvation

(**A**) Lamp1 promoter-luciferase reporter assays. n = 3 technical replicates. (**B**) ChIP assays on the Lamp1 promoter in WT MEFs under normal and GS conditions using anti-USF2 and anti-TFEB antibodies. n = 3 technical replicates. (**C**) A heatmap illustrating expression of differentially expressed genes (DEGs) obtained from RNA-seq results in WT and *Usf2*$^{-/-}$ MEFs under normal and GS conditions. (**D**) A heatmap illustrating expression of DEGs obtained from RNA-seq results of WT and *Usf2*$^{-/-}$ MEFs under normal and AAS conditions. (**E**) ChIP assays on USF2-dependent promoters in WT and Tfeb$^{-/-}$ MEFs under normal and GS conditions. n = 3 technical replicates. * $p<0.05$, ** $p<0.01$, *** $p<0.001$. Statistics by two-tailed t-test.

Phosphorylation of USF2 modulates its DNA-binding activity

I examined the role of USF2 phosphorylation in lysosomal gene repression. Previous studies have shown that USF2 phosphorylation modulates its DNA-binding activity: protein kinase A phosphorylates USF2 in granulosa cells, enhancing its binding to the E-box, and GSK3β phosphorylation increases its DNA binding capacity (Sayasith, Lussier et al. 2005, Horbach, Chi et al. 2014). Under nutrient-rich conditions, USF2 was phosphorylated, and λ-phosphatase treatment reduced its phosphorylation (Fig. III-5A). USF2 phosphorylation occurs at S155 and T230 by GSK3β, and at S222 by CDK5. To further investigate the functional significance of USF2 phosphorylation, I generated the S155A, S222A, and T230A mutants. The S155A mutant almost completely abolished USF2 phosphorylation, while phosphorylation was retained in the S222A and T230A mutants (Fig. III-5B).

Next, I assessed the DNA-binding activity of USF2 by expressing either WT USF2 or the S155A mutant in *Usf2*$^{-/-}$ cells. The S155A mutant exhibited reduced DNA binding to lysosomal gene promoters compared to the WT (Fig. III-5C). When the WT USF2 was expressed, target lysosomal gene mRNA and protein levels were repressed, but no repression was observed with the S155A mutant (Fig. III-5D, E). Similarly, the USF2 knockout-mediated upregulation of lysosomal biogenesis was abolished when WT USF2 was expressed, but not with the S155A mutant (Fig. III-5F, G).

To further understand the impact of USF2 phosphorylation, I generated the phospho-mimetic S155E mutant (Fig. III-5H). In contrast to the S155A mutant, the S155E mutant retained a phosphorylation-mimetic effect, even under glucose starvation. Under these conditions, WT USF2 undergoes dephosphorylation, leading to its dissociation from the promoter and increased TFEB recruitment. However, the S155E mutant failed to dissociate from the promoter, which reduced TFEB recruitment (Fig. III-5I). As a result, TFEB target genes remained inactive even during glucose starvation in the presence of the USF2 S155E mutant (Fig. III-5J). Together, these data suggest that USF2 antagonizes TFEB by binding to the CLEAR motif in a phosphorylation-dependent manner, and that phosphorylation of USF2 at S155 enhances this antagonism.

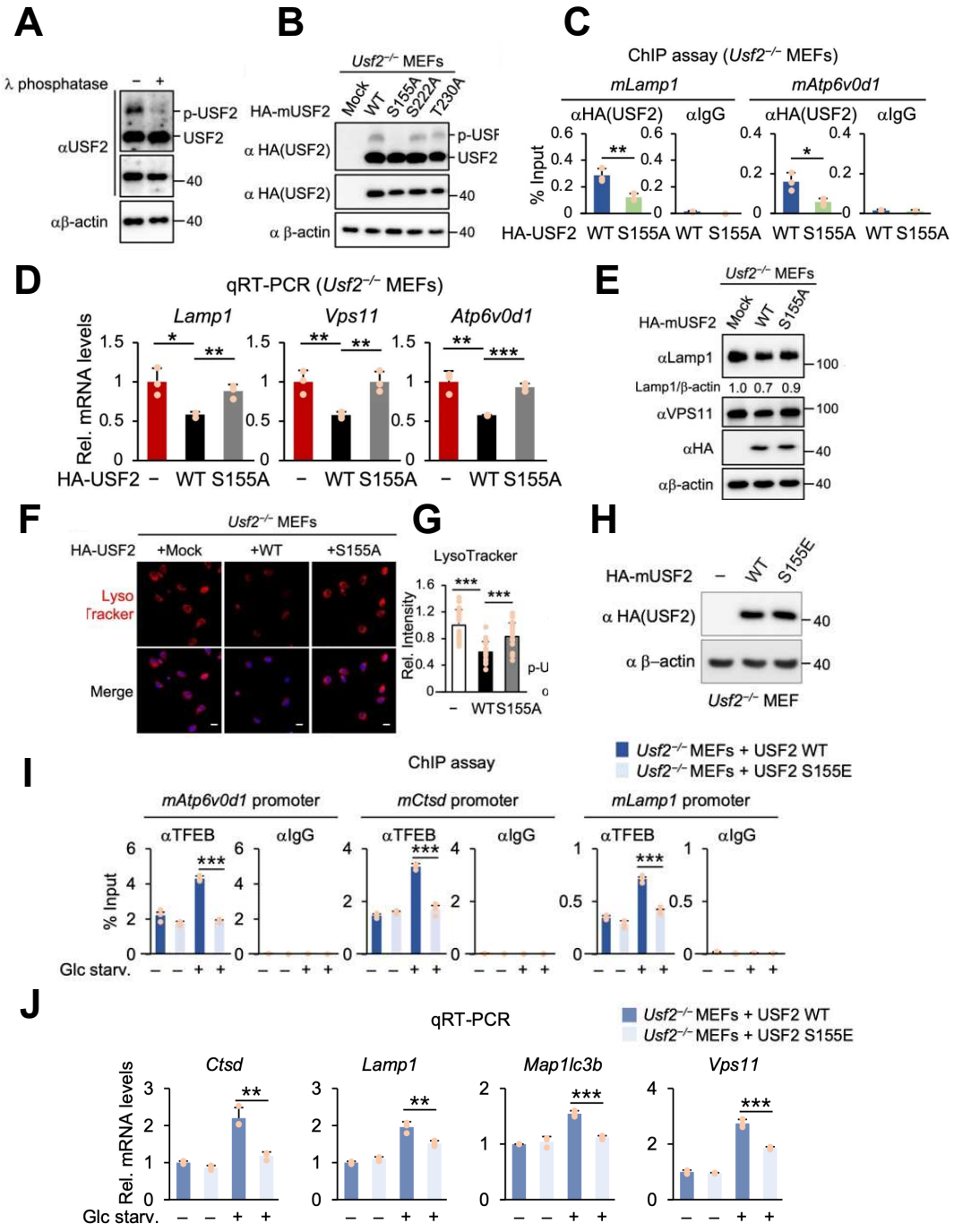
A
λ phosphatase
αUSF2
p-USF2
USF2
αβ-actin
B
Usf2−/− MEFs
HA-mUSF2
Mock
WT
S155A
S222A
T230A
α HA(USF2)
α β-actin
C
ChIP assay (Usf2−/− MEFs)
mLamp1
mAtp6v0d1
αHA(USF2)
αIgG
% Input
HA-USF2 WT S155A WT S155A WT S155A WT S155A
D
qRT-PCR (Usf2−/− MEFs)
Lamp1
Vps11
Atp6v0d1
Rel. mRNA levels
HA-USF2 − WT S155A − WT S155A − WT S155A
E
Usf2−/− MEFs
HA-mUSF2
Mock
WT
S155A
αLamp1
Lamp1/β-actin 1.0 0.7 0.9
αVPS11
αHA
αβ-actin
F
Usf2−/− MEFs
HA-USF2 +Mock +WT +S155A
Lyso Tracker
Merge
G
LysoTracker
Rel. Intensity
− WT S155A
H
HA-mUSF2 − WT S155E
α HA(USF2)
α β–actin
Usf2−/− MEF
I
ChIP assay
Usf2−/− MEFs + USF2 WT
Usf2−/− MEFs + USF2 S155E
mAtp6v0d1 promoter
mCtsd promoter
mLamp1 promoter
αTFEB
αIgG
% Input
Glc starv.
J
qRT-PCR
Usf2−/− MEFs + USF2 WT
Usf2−/− MEFs + USF2 S155E
Ctsd
Lamp1
Map1lc3b
Vps11
Rel. mRNA levels
Glc starv.

Figure III-5. Phosphorylation of USF2 modulates its DNA-binding activity

(**A**) Immunoblot analysis in the presence or absence of λ-phosphatase treatment in WT MEFs. (**B**) Immunoblot analysis using phos-tag™ gel after reconstituting WT, S155A, S222A, and T230A mutants in *Usf2*$^{-/-}$ MEFs. (**C**) ChIP assay on the promoters of lysosomal genes following reconstitution of WT or S155A mutant in *Usf2*$^{-/-}$ MEFs. n = 3 technical replicates. (**D**) qRT-PCR assay of lysosomal genes after reconstituting mock, WT, and S155A mutant in *Usf2*$^{-/-}$ MEFs. n = 3 technical replicates. Mock and USF2 S155A mutant rescued cells were individually compared to USF2 WT rescued cells. (**E**) Immunoblot analysis of lysosomal proteins after reconstituting mock, WT, and S155A mutant in *Usf2*$^{-/-}$ MEFs. (**F**) Representative images of Lysotracker staining in *Usf2*$^{-/-}$ MEFs reconstituted with mock, WT, or S155A mutant. Lysotracker, red; Hoechst, blue. Scale bar, 20 μm. (**G**) Quantification of Lysotracker intensity per cell. Lysotracker assay performed after reconstituting mock, WT, and S155A mutant in *Usf2*$^{-/-}$ MEFs. n = 18 biologically independent samples. Mock and USF2 S155A mutant rescued cells were compared to USF2 WT rescued cells. (**H**) Immunoblot analysis of *Usf2*$^{-/-}$ MEFs along with USF2 WT and USF2 S155E overexpression. (**I**) ChIP assay on USF2-dependent promoters under normal and GS conditions in *Usf2*$^{-/-}$ MEFs with USF2 WT or USF2 S155E reconstitution. n = 3 technical replicates. (**J**) qRT-PCR assay of USF2 target genes under normal and GS conditions in *Usf2*$^{-/-}$ MEFs with USF2 WT or USF2 S155E reconstitution. n = 3 technical replicates. * $p<0.05$, ** $p<0.01$, *** $p<0.001$. Statistics by two-tailed t-test.

GSK3β-dependent Phosphorylation of USF2 regulates its DNA binding

To confirm the role of GSK3β in regulating USF2 phosphorylation, I treated WT MEFs with lithium chloride (LiCl), a well-established pharmacological inhibitor of GSK3β. Immunoblot analysis revealed a significant reduction in USF2 phosphorylation at S155 upon LiCl treatment (Fig. III-6A). This result demonstrated that GSK3β is directly responsible for the phosphorylation of USF2 at this site. Furthermore, the inhibition of GSK3β by LiCl reversed the phosphorylation state of USF2, reinforcing the notion that GSK3β is the primary kinase modulating USF2 phosphorylation under these conditions (Fig. III-6B).

To assess how this phosphorylation impacts the DNA-binding activity of USF2, I conducted ChIP assays targeting the promoters of lysosomal genes. Under normal conditions, USF2 was robustly enriched at these promoters, indicating active binding. However, treatment with LiCl significantly reduced USF2 occupancy on these promoters (Fig. III-6C). This observation suggests that phosphorylation at S155 is essential for USF2 to stably associate with its target DNA regions. The reduced DNA binding upon LiCl treatment highlights the importance of GSK3β-mediated phosphorylation in maintaining USF2's transcriptional repression activity on lysosomal genes.

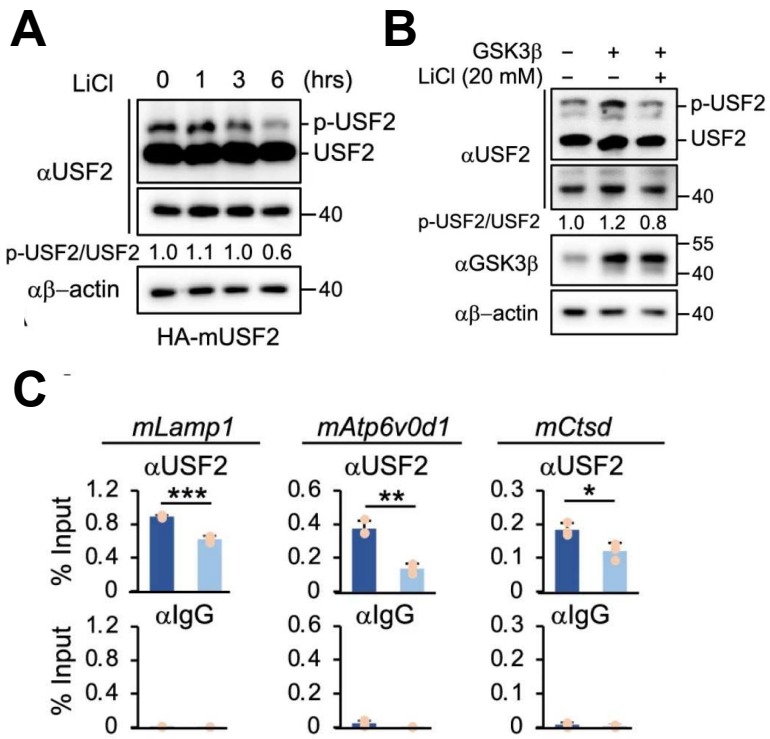

Figure III-6. GSK3β-dependent Phosphorylation of USF2 regulates its DNA binding

(**A**) Immunoblot analysis of USF2 phosphorylation in WT MEFs treated with or without LiCl. (**B**) Immunoblot analysis using phos-tag™ gel under normal, GSK3β-overexpressed, and LiCl-treated conditions. (**C**) ChIP assay for USF2 binding on lysosomal gene promoters in WT MEFs treated with or without LiCl. $n = 3$ technical replicates. * $p<0.05$, ** $p<0.01$, *** $p<0.001$. Statistics by two-tailed t-test.

Nutrient starvation suppresses USF2 phosphorylation via inhibition of GSK3β activity

To elucidate the effects of nutrient starvation on USF2 phosphorylation, I investigated the activity of GSK3β, the key kinase responsible for phosphorylating USF2. Glucose starvation and amino acid starvation significantly reduced USF2 phosphorylation levels, coinciding with decreased GSK3β activity in WT MEFs (Fig. III-7A-D). This finding was corroborated by immunostaining experiments, which revealed increased phosphorylation of GSK3β at serine 9 (S9), a marker of its inactive form, during glucose or amino acid starvation (Fig. III-7E, F).

Notably, under normal conditions, GSK3β phosphorylation at S9 was minimal, allowing the kinase to phosphorylate USF2 efficiently. However, glucose or amino acid starvation induced a significant elevation in S9 phosphorylation, suggesting nuclear inactivation of GSK3β under these conditions. This decrease in GSK3β activity correspondingly led to a marked reduction in USF2 phosphorylation, as observed by immunoblotting with phos-tag™ gels. These results demonstrate a direct link between nutrient availability, GSK3β activity, and USF2 phosphorylation, highlighting a regulatory mechanism by which nutrient starvation modulates USF2-mediated transcriptional activity through GSK3β inhibition.

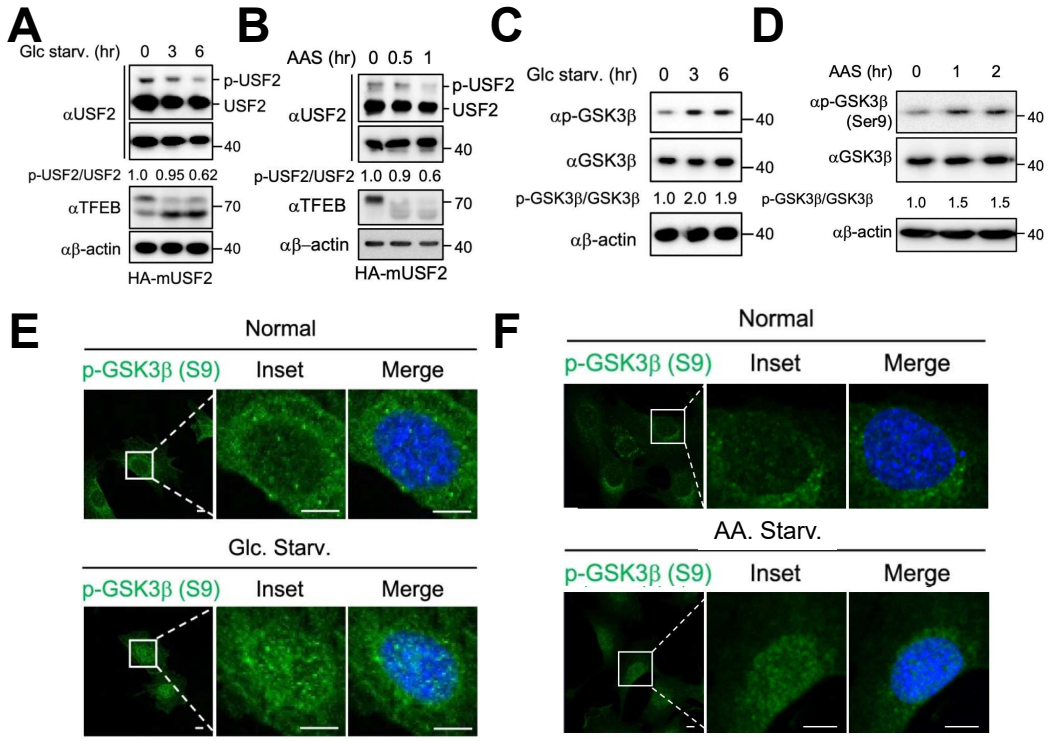

Figure III-7. Nutrient starvation suppresses USF2 phosphorylation via inhibition of GSK3β activity

(**A**) Immunoblot analysis using phos-tag™ gel to detect USF2 phosphorylation under normal and GS conditions in WT MEFs. (**B**) Immunoblot analysis using phos-tag™ gel for USF2 phosphorylation in WT MEFs under normal and AAS conditions. (**C**) Immunoblot analysis of GSK3β phosphorylation (Ser9) under normal and GS conditions in WT MEFs, indicating GSK3β inhibition. (**D**) Immunoblot analysis of GSK3β phosphorylation (Ser9) under normal and AAS conditions in WT MEFs, indicating GSK3β inhibition. (**E**) Representative confocal microscopy images showing GSK3β Ser9 phosphorylation (inactive form) under normal and GS conditions. Phosphorylated GSK3β (Ser9) is shown in green; nuclei are counterstained with DAPI (blue). Scale bar, 10 μm. (**F**) Confocal microscopy images of GSK3β Ser9 phosphorylation under normal and AAS conditions. Phosphorylated GSK3β (Ser9) is shown in green; nuclei are counterstained with DAPI (blue). Scale bar, 10 μm.

USF2 promotes clearance of misfolded α1-antitrypsin aggregates

To investigate the role of USF2 in lysosomal biogenesis and its implications in protein aggregate clearance, I analyzed *Usf2*$^{-/-}$ mouse embryos and HepG2 cells. Immunofluorescence analysis revealed that *Usf2*$^{-/-}$ mouse embryos exhibit increased Lamp1 expression, particularly in liver tissue, indicating enhanced lysosomal biogenesis (Fig. III-8A). This suggests that USF2 serves as a repressor of lysosomal activity, with significant implications for liver function and pathology.

To further explore the physiological consequences of USF2 deficiency, I used a model of ATZ aggregation. ATZ is a misfolded protein that accumulates in the endoplasmic reticulum (ER) of hepatocytes, causing ER stress, liver damage, and potential progression to cirrhosis or hepatocellular carcinoma. While soluble ATZ monomers are primarily degraded by the proteasome via ER-associated protein degradation (ERAD), aggregated ATZ relies on autophagy and lysosomal pathways for clearance.

In GFP-ATZ-overexpressing HepG2 cells, USF2 knockdown via siRNA significantly enhanced lysosomal biogenesis and reduced GFP-ATZ protein levels (Fig. III-8B). Confocal microscopy further demonstrated decreased ATZ aggregates in USF2-deficient cells (Fig. III-8C). Inhibition of lysosomal activity using BafA1 largely restored ATZ levels in USF2-knockdown cells (Fig. III-8D, E), confirming that the degradation is lysosome-dependent.

Immunocytochemical analysis showed increased LAMP1 staining intensity in USF2-

knockdown cells compared to control cells, regardless of BafA1 treatment (Fig. III-8F), confirming enhanced lysosome biogenesis. Furthermore, ATZ aggregates were efficiently cleared in the absence of BafA1 but accumulated upon BafA1 treatment, co-localizing with lysosomes (Fig. III-8G, H). These findings suggest that USF2 knockdown promotes the degradation of ATZ aggregates through a lysosome-mediated pathway.

Taken together, these results highlight a important role for USF2 in repressing lysosomal activity and suggest that targeting USF2 may offer therapeutic potential for diseases characterized by protein aggregation, such as α1-antitrypsin deficiency. Enhanced lysosomal function via USF2 inhibition could provide an effective strategy to alleviate the pathological consequences of misfolded protein accumulation.

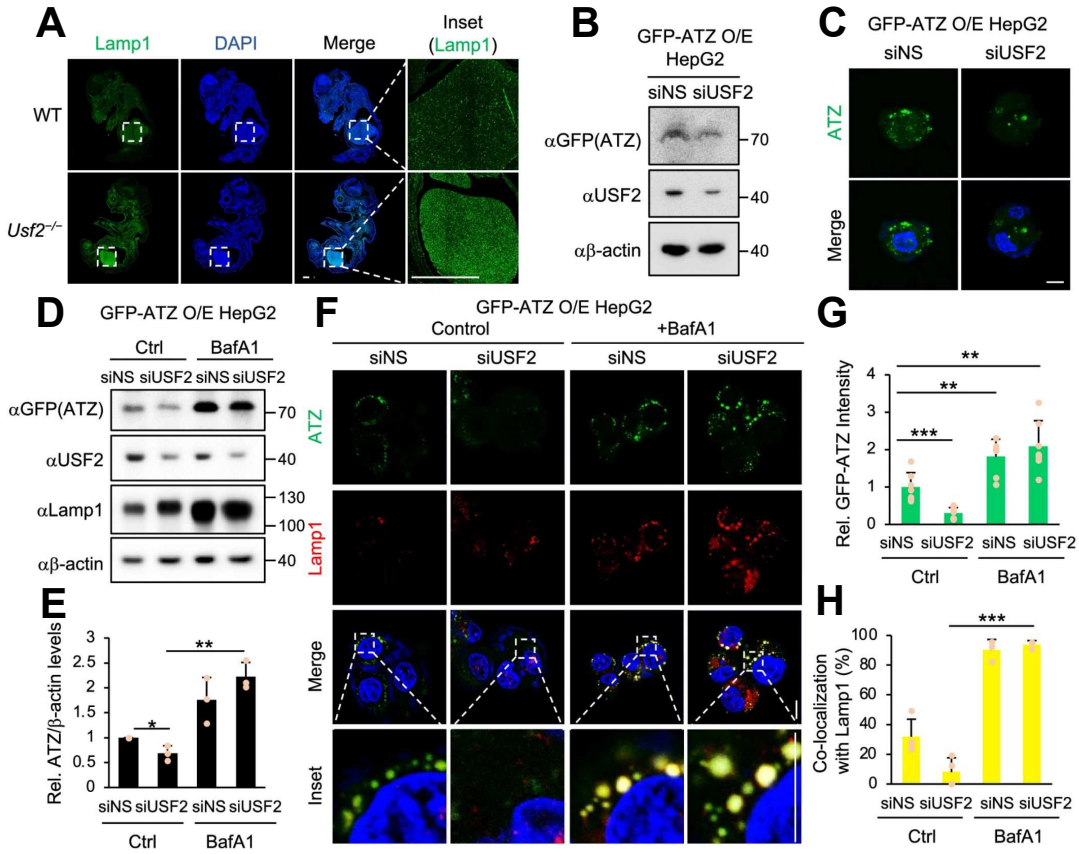

Figure III-8. USF2 promotes clearance of misfolded α1-antitrypsin aggregates

(**A**) Immunofluorescence of Lamp1 (green) in liver sections from 16.5-day-old WT and *Usf2*$^{-/-}$ embryos. Nuclei stained with Hoechst (blue). Scale bar, 1 mm. (**B**) Immunoblot of GFP-ATZ in GFP-ATZ O/E HepG2 cells transfected with siNS or siUSF2. (**C**) Confocal images of GFP-ATZ aggregates in GFP-ATZ O/E HepG2 cells with siNS or siUSF2. Scale bar, 10 μm. (**D**) Immunoblot of GFP-ATZ in GFP-ATZ O/E HepG2 cells with siNS or siUSF2, with or without BafA1 treatment. (**E**) Quantification of GFP-ATZ levels normalized to β-actin in cells from (D). Data are mean ± SEM, n = 3. (**F**) Confocal images of GFP-ATZ (green), Lamp1 (red), and nuclei (blue) in GFP-ATZ O/E HepG2 cells treated with siNS or siUSF2, with or without BafA1. Scale bar, 10 μm. (**G**) Quantification of GFP-ATZ fluorescence intensity in cells from (F). (**H**) Quantification of Lamp1 and GFP-ATZ co-localization in cells from (F). Data are mean ± SEM, n = 3. * $p<0.05$, ** $p<0.01$, *** $p<0.001$. Statistics by two-tailed t-test.

Synergistic effects of TFEB overexpression and USF2 knockdown on ATZ degradation

I further explored the synergistic effects of TFEB overexpression and USF2 knockdown on the degradation of ATZ aggregates. Previous studies suggested that TFEB overexpression could enhance lysosomal gene activation and, in turn, promote the degradation of protein aggregates, including ATZ. In our study, I observed that TFEB overexpression significantly increased lysosomal gene expression and facilitated ATZ degradation (Pastore, Blomenkamp et al. 2013). Notably, when USF2 was knocked down in the context of TFEB overexpression, GFP-ATZ levels (Fig. III-9A, B) and ATZ aggregates (Fig. III-9C, D) were further reduced, demonstrating a synergistic effect between TFEB activation and USF2 depletion in enhancing ATZ degradation.

This enhanced degradation was associated with increased autophagy and lysosomal biogenesis, as shown by the upregulation of lysosomal proteins and markers of autophagic flux. These findings suggest that USF2 inhibition potentiates the effects of TFEB activation, leading to a more efficient clearance of ATZ aggregates. The combined approach of activating TFEB and inhibiting USF2 may offer a promising therapeutic strategy for diseases involving intracellular protein aggregation, such as α1-antitrypsin deficiency, by leveraging the cell's autophagy and lysosomal pathways.

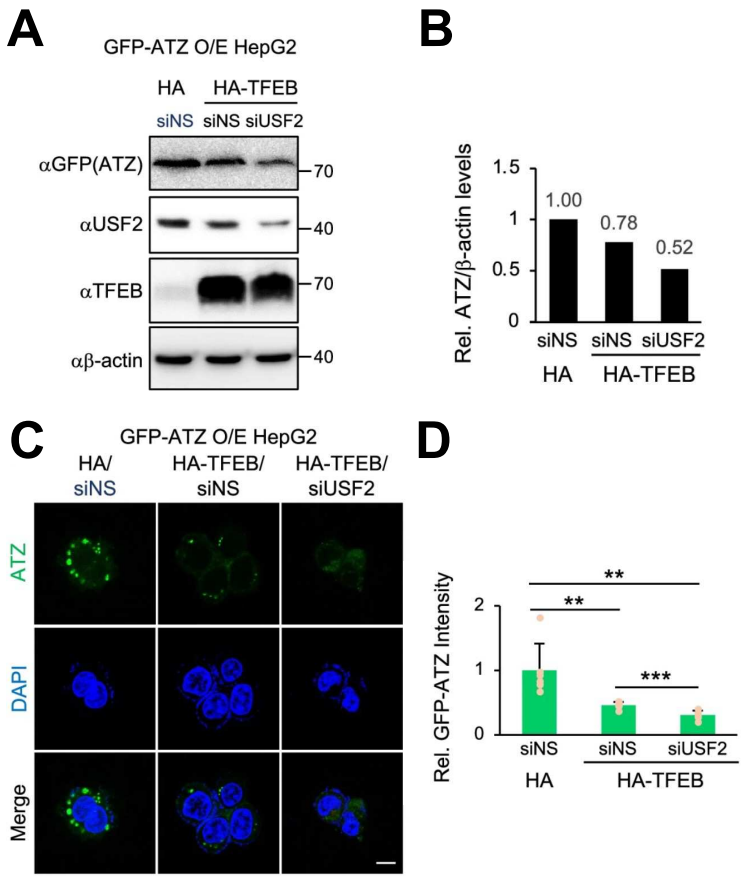

Figure III-9. Synergistic effects of TFEB overexpression and USF2 knockdown on ATZ degradation

(**A**) Immunoblot analysis of GFP-ATZ O/E HepG2 cell lines after TFEB overexpression and USF2 knockdown. (**B**) Quantification of GFP-ATZ protein levels relative to β-actin in GFP-ATZ O/E HepG2 cell lines after TFEB overexpression and USF2 knockdown. (**C**) Representative confocal images of GFP-ATZ O/E HepG2 cell lines after TFEB overexpression and USF2 knockdown. Scale bar, 10 μm. (**D**) Quantification of GFP-ATZ intensity. n = 5 biologically independent samples. siNS and siNS+HA-TFEB cells were compared to siUSF2+HA-TFEB cells. * $p<0.05$, ** $p<0.01$, *** $p<0.001$. Statistics by two-tailed t-test.

III-4. Discussion

Autophagy and lysosomal biogenesis are tightly regulated processes essential for cellular homeostasis, particularly under nutrient-starvation conditions. My study highlights the pivotal role of USF2 as a transcriptional repressor and its competitive interplay with MiT/TFE family members, such as TFEB, in modulating the expression of autophagy- and lysosome-related genes.

Motif analysis revealed that USF2 preferentially binds to the E-box motif (5′-GTCACGTG-3′), a site also targeted by MiT/TFE family members. This overlapping motif suggests potential competition between USF2 and MiT/TFE factors for promoter occupancy. Indeed, ChIP-seq data confirmed the co-localization of USF2 with TFE3 and MITF at genomic regions regulating genes like *Lamp1*, *Vps11*, *Atp6v0d1*, and *Gaa*. Functional analyses demonstrated that *Usf2*-knockout cells exhibit increased recruitment of TFEB to these target promoters, leading to enhanced expression of autophagy-related genes. Furthermore, transcription factor enrichment and perturbation analyses indicated that the gene expression patterns repressed by USF2 align closely with those activated by TFEB overexpression, reinforcing the antagonistic regulation between these factors.

Interestingly, USF2 does not appear to influence the nuclear translocation of TFEB, as glucose starvation induced comparable TFEB localization between WT and *Usf2*$^{-/-}$ cells. Instead, USF2 competes with TFEB at the promoter level. Under steady-state conditions, USF2 binds to autophagy gene promoters and represses their expression, while TFEB remains primarily cytoplasmic. However, during glucose or amino acid starvation, TFEB

translocates to the nucleus and displaces USF2 from its target promoters, resulting in transcriptional activation. Luciferase reporter assays confirmed that USF2 suppresses TFEB-induced gene activation in a DNA-binding-dependent manner, further establishing USF2 as a direct competitor of TFEB.

The regulatory role of USF2 is also modulated by its phosphorylation status. Under nutrient-rich conditions, USF2 phosphorylation enhances its DNA-binding activity, mediated by kinases such as GSK3β. Nutrient starvation inhibits GSK3β activity, leading to reduced USF2 phosphorylation and diminished DNA-binding capacity. This dynamic regulation allows TFEB to dominate under starvation conditions, facilitating the activation of lysosomal and autophagy-related genes. Moreover, the increased recruitment of TFEB to promoters in *Usf2*-deficient cells correlates with elevated H3K27ac levels, underscoring the epigenetic changes associated with TFEB-driven transcription.

To further explore the physiological relevance of USF2 in lysosomal biogenesis, I investigated the effects of USF2 deficiency in cellular models. In *Usf2*$^{-/-}$ mouse embryos, particularly in liver tissue, I observed increased expression of Lamp1, a marker of lysosomal biogenesis, suggesting enhanced lysosomal activity. Additionally, USF2-deficient cells exhibited a more efficient clearance of protein aggregates, specifically ATZ aggregates, a hallmark of liver disease. USF2 knockdown in GFP-ATZ-overexpressing HepG2 cells promoted lysosomal biogenesis and reduced ATZ levels without altering mRNA expression, indicating that the observed effects were post-transcriptional. Moreover, inhibiting lysosomal activity with BafA1 restored ATZ accumulation, confirming the

lysosome-dependent nature of the degradation process.

These findings were further strengthened by our exploration of TFEB overexpression in the context of USF2 knockdown. I observed that TFEB activation significantly enhanced lysosomal gene expression and facilitated the degradation of ATZ aggregates. The combination of TFEB overexpression and USF2 depletion resulted in a further reduction of GFP-ATZ levels and ATZ aggregates, demonstrating a synergistic effect between these two factors in promoting protein clearance. This was associated with increased autophagy and lysosomal biogenesis, suggesting that USF2 inhibition potentiates the effects of TFEB, leading to enhanced protein degradation.

In conclusion, USF2 acts as a transcriptional repressor that competes with TFEB for binding to autophagy- and lysosome-related gene promoters, thus modulating lysosomal function. Its activity is regulated by nutrient availability and phosphorylation status, allowing it to function as a key repressor of lysosomal biogenesis. Targeting USF2 to enhance lysosomal activity and autophagic flux holds therapeutic potential for diseases characterized by protein aggregation, such as α1-antitrypsin deficiency, by promoting the efficient clearance of misfolded proteins.

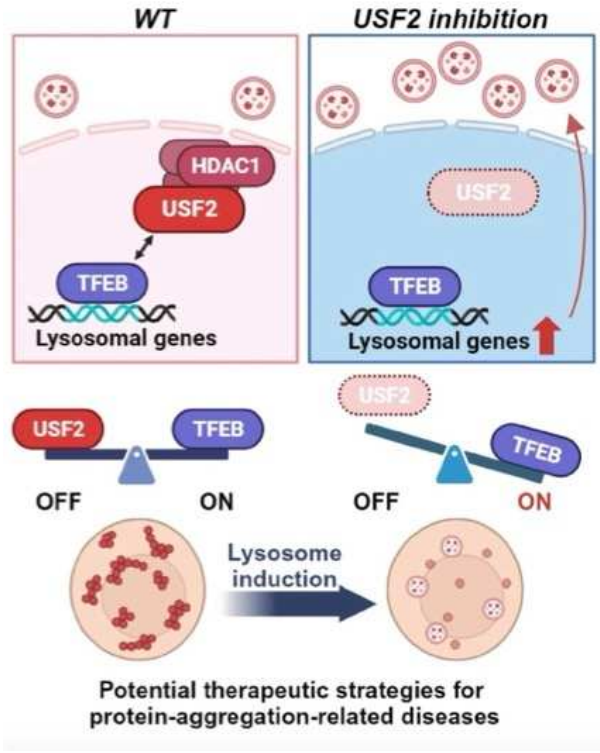

Figure III-10. Schematics of Therapeutic Strategies for α1-Antitrypsin Deficiency through the Inhibition of USF2 and the Activation of TFEB

Inhibiting the repressor activity of USF2 or enhancing the activator function of TFEB can promote lysosomal and autophagy activation, leading to the degradation of ATZ aggregates. Furthermore, the combined application of both approaches may produce a synergistic effect.

III-5. Materials and Methods

Reagents

The following commercially available antibodies were used; anti-USF2 (ab125184, Abcam), anti-TFEB (ab2636, Abcam), anti-HDAC1 (C15410325-50, Diagenode), anti-CTSD (sc-377299, Santa Cruz), anti-ATP6V0D1 (ab202897, Abcam), anti-VPS11 (ab125083, Abcam), anti-Lamp1 (ab24170, Abcam), anti-LC3 (ab48394, ab51520, Abcam), anti-SQSTM1/p62 (ab101266, Abcam), anti-H3K27Ac (ab4729, Abcam), anti-GSK3β (sc-81462, Santa Cruz), anti-Phospho-GSK3β (Ser9) (9323, Cell Signaling Technology) and anti-β-actin (A1978, Sigma-Aldrich). The following chemicals were used in this study; Bafilomycin A1 (11038, Sigma), Lysosensor (L7535, Thermo Fisher Scientific), Lysotracker Green (L7526, Thermo Fisher Scientific), Lysotracker Red (L7528, Thermo Fisher Scientific) and DQ Red BSA (D12051, Thermo Fisher Scientific).

Cell culture and transfection

Cells were cultured at 37 °C in Dulbecco's modified Eagle's medium (DMEM) containing 10 % fetal bovine serum (FBS) and antibiotics in a humidified incubator with 5 % CO_2. All cell lines were tested for mycoplasma contamination. For glucose starvation, cells were washed with DPBS and incubated with glucose-free DMEM supplemented with 10 % dialyzed FBS. Transfection was performed using Lipofectamine 3000 (L3000075, Invitrogen) according to the manufacturer's protocol.

Generation of *Usf2* $^{-/-}$ mice and MEFs

Usf2 mutant mice were generated by introducing the gRNA/Cas9 RNP solution into fertilized eggs from the mating of B6D2F1 mice, as previously described (Noda, Sakurai et al. 2019). The gRNA sequences used were 5′-GAGCCGCTTGCGCTGATCAC-3′ and 5′-GCTCTTCTTCTCTCATCTCG-3′. By mating the resulting *Usf2*$^{+/-}$ mice (founder generation) with wild-type mice, I established *Usf2* mutant mice with a 2112 bp deletion in the *Usf2* gene. Frozen spermatozoa from B6D2-*Usf2*, RBRC#11002, and CARD#2909 will be available through RIKEN BRC (http://en.brc.riken.jp/index.shtml) and CARD R-BASE (https://cardmice.com/rbase/). All animal experiments were conducted under protocols approved by the Institutional Animal Care and Use Committee (IACUC) of Seoul National University (SNU-200901-5-3).

WT and *Usf2*$^{-/-}$ MEFs were generated by crossing two *Usf2*$^{+/-}$ mice. The pregnant female *Usf2*$^{+/-}$mice were euthanized at 13.5 days post-coitum (dpc). The embryos were dissected by removing their heads, limbs, gonads, tail, and other visceral masses. The embryos were then chopped and digested with 0.25 % trypsin/ethylenediaminetetraacetic acid (EDTA). The enzymatic activity was neutralized by adding DMEM with 10 % FBS and antibiotics. The tissues were pipetted up and down to obtain a single-cell suspension. The cells were cultured in 100 mm culture dishes until 70–80 % confluency and sub-cultured at a ratio of 1:4. MEFs were used at different passages (P1–10).

Preparation of whole-cell lysates

All cells were briefly rinsed with cold PBS before harvesting. For whole-cell lysates, the cells were resuspended in RIPA buffer (150 mM NaCl, 1 % Triton X-100, 1 % sodium deoxycholate, 0.1 % SDS, 50 mM Tris-HCl [pH 7.5], and 2 mM EDTA) supplemented with protease inhibitors and sonicated using a Branson Sonifier 450 at output 3 and a duty cycle of 30 for five pulses. For the cytosolic and nuclear fractions, cells were lysed in harvest buffer (10 mM HEPES [pH 7.9], 50 mM NaCl, 0.5 M sucrose, 0.1 mM EDTA, 0.5 % Triton X-100, DTT, PMSF, and protease inhibitors), incubated on ice for 5 min, and centrifuged at 120 × *g* for 10 min at 4 °C. The supernatant (cytosolic fraction) was transferred into a separate tube. The nuclear pellet was rinsed twice with 500 µl of buffer A (10 mM HEPES [pH 7.9], 10 mM KCl, 0.1 mM EDTA, and 0.1 mM EGTA) and centrifuged at 120 × *g* for 10 min at 4 °C. The supernatant was discarded, and the pellet (nuclear fraction) was resuspended in RIPA buffer and sonicated. All lysates were quantified using the Bradford method and analyzed by SDS–PAGE.

Immunofluorescence analysis

Immunocytochemistry was performed as described previously (Shin, Kim et al. 2016). Cells grown on coverslips at a density of 3×10^4 cells/well in a 12-well plate were washed with PBS and fixed with 2 % formaldehyde in PBS for 10 min at room temperature. Fixed cells were permeabilized with 0.5 % Triton X-100 in PBS (PBS-T) and blocking step was performed with 3 % bovine serum albumin (BSA) in PBS-T for 1 h. Cells were incubated with antibodies overnight at 4 °C, followed by incubation with fluorescently labeled secondary antibodies for 1 h (Invitrogen), and mounted and visualized under a confocal

microscope (Zeiss, LSM700). For autophagy studies, MEFs were cultured in complete medium or glucose-starved medium for 24 h.

Lysotracker and Lysosensor assays

Cells were stained with 500 nM Lysotracker Green (L7526, Thermo Fisher Scientific), Lysotracker Red (L7528, Thermo Fisher Scientific) or Lysosensor (L7535, Thermo Fisher Scientific) for 4 h (25 °C, 5 % CO_2). After washing with the probe-free medium, the samples were observed using a confocal microscope (Zeiss, LSM 700).

Quantitative RT-PCR

All Total RNA was extracted using Trizol (15596026, Invitrogen), and reverse transcription was performed from 1 μg of total RNA using an SRK-1000 SuPrimeScript cDNA Synthesis Kit (Genet Bio, Daejeon, Republic of Korea). The abundance of mRNAs was detected using an ABI prism 7500 system or BioRad CFX384 with SYBR TOPreal qPCR 2× PreMix (RT500, Enzynomics). The amount of mRNA was calculated using the ΔΔCt method, and *Hprt* was used as a control. All reactions were performed in triplicates. The following mouse primers were used in this study;

Ctsd; forward (fwd) 5′- TAAGACCACGGAGCCAGTGTCA-3′,

reverse (rev) 5′- CCACAGGTTAGAGGAGCCAGTA-3′;

Atp6v0d1; forward (fwd) 5′- GCATCTCAGAGCAGGACCTTGA-3′,

reverse (rev) 5′- GGATAGGACACATGGCATCAGC-3′;

Vps11; forward (fwd) 5′- ATCGGCAGTCTCTGGCTAATGC-3′,

reverse (rev) 5′- GGACCTTGATGGCTGTCTCTAC-3′;

Lamp1; forward (fwd) 5′- CCAGGCTTTCAAGGTGGACAGT-3′,

reverse (rev) 5′- GGTAGGCAATGAGGACGATGAG-3′;

Map1lc3b; forward (fwd) 5′- GTCCTGGACAAGACCAAGTTCC-3′,

reverse (rev) 5′- CCATTCACCAGGAGGAAGAAGG-3′;

ChIP and qRT–PCR analyzes

ChIP assays were performed as previously described (Shin, Kim et al. 2016). Cells were cross-linked in 1 % formaldehyde for 10 min and washed with ice-cold PBS three times. After glycine quenching for 5 min, the cells were collected and lysed in a buffer containing 50 mM Tris–HCl (pH 8.1), 10 mM EDTA, and 1 % SDS, supplemented with a complete protease inhibitor cocktail (11873580001, Roche). After DNA fragmentation through sonication, chromatin extracts containing DNA fragments with an average of 250 bp were then diluted ten times with dilution buffer containing 1 % Triton X-100, 2 mM EDTA, 150 mM NaCl, and 20 mM Tris–HCl (pH 8.1) with complete protease inhibitor cocktail and subjected to immunoprecipitations overnight at 4 °C. Immunocomplexes were captured by incubating 40 µl of protein A/G Sepharose for 1.5 h at 4 °C. Beads were washed with TSE I buffer (0.1 % SDS, 1 % Triton X-100, 2 mM EDTA, 20 mM Tris–HCl (pH 8.1), and 150 mM NaCl), TSE II buffer (0.1 % SDS, 1 % Triton X-100, 2 mM EDTA, 20 mM Tris–

HCl (pH 8.1), and 500 mM NaCl), buffer III (0.25 M LiCl, 1 % NP-40, 1 % deoxycholate, 10 mM Tris–HCl (pH 8.1), and 1 mM EDTA), three times TE buffer (10 mM Tris–HCl (pH 8.0) and 1 mM EDTA) and eluted in elution buffer (1 % SDS and 0.1 M $NaHCO_3$). The supernatant was incubated overnight at 65 °C to reverse crosslink and then digested with RNase A for 1 h at 37 °C and proteinase K for 2 h at 55 °C. ChIP and input DNA were then purified and analyzed for qRT–PCR analysis or used for constructing sequencing libraries. The following primers were used;

Atp6v0d1; forward (fwd) 5′- CAACTAGACTCCCCGGATCA-3′,

reverse (rev) 5′- GTCGGGCACTCCAGAGTAA-3′;

Lamp1; forward (fwd) 5′- GTGGGGAGAGGGCAAGATA-3′,

reverse (rev) 5′- CGCCAGCTTACTCCTCACTT−3′;

Vps11; forward (fwd) 5′- TCCTTCACCAGCTCCTTCTC-3′,

reverse (rev) 5′- GAGCAGCAAGCCTTTTGTG-3′;

Ctsd; forward (fwd) 5′- CGGCTTATAGGCAGGATGAC-3′,

reverse (rev) 5′- GTGCGTAGGCCTGGAGTAGG-3′;

Immunohistochemistry

WT and *Usf2*$^{-/-}$ embryos were fixed in 10 % formalin (HT5011, Sigma) overnight at 4 °C. Tissues were sequentially dehydrated in ethanol at concentrations ranging from 50 % to 100 %. Dehydrated specimens were subsequently infiltrated with 100 % xylene and embedded in paraffin wax. For immunostaining, tissues were sectioned at 7 μm thickness

and blocked with 5 % BSA. Sections were then stained with the primary antibodies for 4 h at 25 °C. For the secondary reaction, Alexa Fluor 488-labeled secondary antibodies were used, and sections were mounted with DAPI (D9542, Sigma). The mounted sections were visualized under a confocal microscope (LSM700, Zeiss)

Transfection of siRNA

LipofectamineTM 3000 transfection reagent kit (Invitrogen, L3000001) was used according to the manufacturer's protocol to transfect siRNA targeting the gene to cells. Lipofectamine 3000-siRNA complex was initially generated in volume ratio of 2:1 and mixed and incubated for 15 min at room temperature. The mixture was then added onto cells in culture dish in confluency of 70–80% for 6 h in final siRNA concentration of 20 nM. The Lipofectamine complex was washed out after 6 h with fresh media and culture overnight. The following sequences of siRNA were used;

si*Tfeb*; 5'-GCAGGCTGTCATGCATTATAT-3',

si*USF2*; 5'-TCCTCCACTTGGAAACGGTAT-3'.

Statistical analysis

Experiments were performed independently at least three times. Random images were chosen for Lysotracker and DQ red BSA intensity counting. Lysotracker and DQ red BSA staining intensity was measured using ImageJ. *P* values were calculated using two-tailed *t*-tests. For animal studies, sample size was determined empirically based on previous studies to ensure appropriate statistical power. Mice were randomly chosen for fasting. No animals

were excluded from statistical analysis, and the investigators were not blinded to the study. Values are expressed as mean ± SD. Significance was analyzed using a two-tailed, unpaired *t*-test. Statistical significance was set at $p < 0.05$.

CHAPTER IV
Conclusion

Autophagy is known to be tightly regulated by an intricate network of transcriptional and epigenetic mechanisms that adapt to various cellular conditions. Transcription factors such as TFEB and FOXO3a, along with chromatin modifiers, play pivotal roles in orchestrating autophagic gene expression. Despite significant advances in understanding transcriptional activation during autophagy, the mechanisms of transcriptional repression and their balance with activation remain poorly understood.

This study explored the role of USF2, a transcriptional repressor, in regulating autophagy and lysosomal biogenesis. USF2's ability to interact with chromatin modifiers, particularly the NuRD complex, was investigated to elucidate its role in the transcriptional suppression of autophagy-related genes. Phosphorylation by GSK3β emerged as a critical regulator of USF2's DNA-binding affinity and transcriptional activity. Disruption of this modification led to diminished USF2 function, revealing a key pathway by which cellular stress responses modulate autophagic gene expression.

My findings also highlighted the competitive interplay between USF2 and TFEB, demonstrating how their dynamic regulation ensures a finely tuned autophagic response to varying environmental cues. While TFEB primarily activates lysosomal and autophagic genes under nutrient-starved conditions, USF2 counterbalances this activation to maintain homeostasis, preventing excessive autophagy that could lead to cellular dysfunction.

Furthermore, the discovery of post-translational modifications of USF2, such as phosphorylation and potential acetylation, provides new insights into how these modifications regulate its interaction with other transcriptional regulators and chromatin

modifiers. This nuanced regulatory mechanism may extend to other physiological contexts, such as oxidative stress or aging, where autophagy plays a protective role.

My intriguing extension of this study is the application of our findings to disease contexts such as alpha-1-antitrypsin deficiency (AATD), where misfolded protein aggregates are cleared via autophagy. The competitive dynamics between USF2 and TFEB could offer therapeutic opportunities to selectively modulate autophagy pathways, potentially mitigating disease progression.

My work underscores the importance of transcriptional repressors in the broader regulatory landscape of autophagy. By delineating the roles of USF2 and its interplay with TFEB, this study not only provides a deeper understanding of autophagic regulation but also opens avenues for targeted therapeutic strategies in age-related diseases, cancer, and neurodegenerative disorders. Future investigations should focus on identifying additional co-factors and chromatin remodeling complexes involved in this process. Moreover, pharmacological modulation of transcription factors like USF2 and TFEB, alongside their associated post-translational modifications, represents a promising area for developing precision therapies.

In conclusion, this research bridges significant gaps in our understanding of autophagy regulation, highlighting the interplay between transcriptional activation and repression. By uncovering the molecular mechanisms underlying USF2's role, it provides a foundation for future studies that could unravel further complexities of autophagic regulation and its implications for human health.

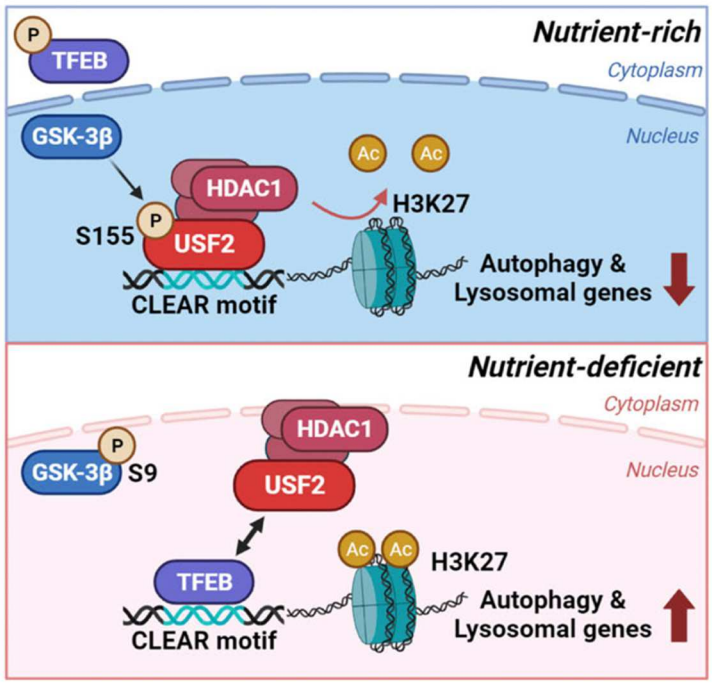

Figure IV-1. Schematics of the regulation of autophagy and lysosome genes by USF2 and TFEB under nutrient-rich or deficient condition

USF2 acts as a transcriptional repressor that antagonizes TFEB by competing for binding motifs on autophagy- and lysosome-related gene promoters. This competition is dynamically regulated by nutrient availability, with phosphorylation-dependent modulation of USF2 activity.

REFERENCES

Allen, H. F., P. A. Wade and T. G. Kutateladze (2013). The nurd architecture. Cellular and Molecular Life Sciences, *70*, 3513-3524.

Ballabio, A. and J. S. Bonifacino (2020). Lysosomes as dynamic regulators of cell and organismal homeostasis. Nature reviews Molecular cell biology, *21*, 101-118.

Broz, D. K., S. S. Mello, K. T. Bieging, D. Jiang, R. L. Dusek, C. A. Brady, A. Sidow and L. D. Attardi (2013). Global genomic profiling reveals an extensive p53-regulated autophagy program contributing to key p53 responses. Genes & development, *27*, 1016-1031.

Casado, M., V. S. Vallet, A. Kahn and S. Vaulont (1999). Essential role in vivo of upstream stimulatory factors for a normal dietary response of the fatty acid synthase gene in the liver. Journal of Biological Chemistry, *274*, 2009-2013.

Chang, L. A., T. Smith, P. Pognonec, R. G. Roeder and H. Murialdo (1992). Identification of USF as the ubiquitous murine factor that binds to and stimulates transcription from the immunoglobulin λ2 chain promoter. Nucleic acids research, *20*, 287-293.

Cogswell, J. P., M. M. Godlevski, M. Bonham, J. Bisi and L. Babiss (1995). Upstream stimulatory factor regulates expression of the cell cycle-dependent cyclin B1 gene promoter. Molecular and cellular biology.

Corre, S. and M. D. Galibert (2005). Upstream stimulating factors: highly versatile stress-responsive transcription factors. Pigment cell research, *18*, 337-348.

Corre, S., A. Primot, E. Sviderskaya, D. C. Bennett, S. Vaulont, C. R. Goding and M.-D. Galibert (2004). UV-induced expression of key component of the tanning process, the

POMC and MC1R genes, is dependent on the p-38-activated upstream stimulating factor-1 (USF-1). Journal of Biological Chemistry, *279*, 51226-51233.

Cox, D. W. and G. D. Billingsley (1989). Rare deficiency types of alpha 1-antitrypsin: electrophoretic variation and DNA haplotypes. American journal of human genetics, *44*, 844.

Eijkelenboom, A. and B. M. Burgering (2013). FOXOs: signalling integrators for homeostasis maintenance. Nature reviews Molecular cell biology, *14*, 83-97.

Eriksson, S., J. Carlson and R. Velez (1986). Risk of cirrhosis and primary liver cancer in alpha1-antitrypsin deficiency. New England journal of medicine, *314*, 736-739.

Füllgrabe, J., G. Ghislat, D.-H. Cho and D. C. Rubinsztein (2016). Transcriptional regulation of mammalian autophagy at a glance. Journal of cell science, *129*, 3059-3066.

Galibert, M. D., S. Carreira and C. R. Goding (2001). The Usf-1 transcription factor is a novel target for the stress-responsive p38 kinase and mediates UV-induced Tyrosinase expression. The EMBO Journal.

Gao, E., Y. Wang, J. L. Alcorn and C. R. Mendelson (2003). Transcription factor USF2 is developmentally regulated in fetal lung and acts together with USF1 to induce SP-A gene expression. American Journal of Physiology-Lung Cellular and Molecular Physiology, *284*, L1027-L1036.

Gelling, C. L., I. W. Dawes, D. H. Perlmutter, E. A. Fisher and J. L. Brodsky (2012). The endosomal protein-sorting receptor sortilin has a role in trafficking α-1 antitrypsin. Genetics, *192*, 889-903.

Gosai, S. J., J. H. Kwak, C. J. Luke, O. S. Long, D. E. King, K. J. Kovatch, P. A. Johnston,

T. Y. Shun, J. S. Lazo and D. H. Perlmutter (2010). Automated high-content live animal drug screening using C. elegans expressing the aggregation prone serpin α1-antitrypsin Z. PloS one, *5*, e15460.

Horbach, T., T. F. Chi, C. Götz, S. Sharma, A. H. Juffer, E. Y. Dimova and T. Kietzmann (2014). GSK3β-dependent phosphorylation alters DNA binding, transactivity and half-life of the transcription factor USF2. PLoS One, *9*, e107914.

Kamimoto, T., S. Shoji, T. Hidvegi, N. Mizushima, K. Umebayashi, D. H. Perlmutter and T. Yoshimori (2006). Intracellular inclusions containing mutant α1-antitrypsin Z are propagated in the absence of autophagic activity. Journal of Biological Chemistry, *281*, 4467-4476.

Kelly, R. D. and S. M. Cowley (2013). The physiological roles of histone deacetylase (HDAC) 1 and 2: complex co-stars with multiple leading parts. Biochemical Society Transactions, *41*, 741-749.

Klionsky, D. J. and S. D. Emr (2000). Autophagy as a regulated pathway of cellular degradation. Science, *290*, 1717-1721.

Kruse, K. B., A. Dear, E. R. Kaltenbrun, B. E. Crum, P. M. George, S. O. Brennan and A. A. McCracken (2006). Mutant fibrinogen cleared from the endoplasmic reticulum via endoplasmic reticulum-associated protein degradation and autophagy: an explanation for liver disease. The American journal of pathology, *168*, 1299-1308.

Lapierre, L. R., C. Kumsta, M. Sandri, A. Ballabio and M. Hansen (2015). Transcriptional and epigenetic regulation of autophagy in aging. Autophagy, *11*, 867-880.

Le Guezennec, X., M. Vermeulen, A. B. Brinkman, W. A. Hoeijmakers, A. Cohen, E.

Lasonder and H. G. Stunnenberg (2006). MBD2/NuRD and MBD3/NuRD, two distinct complexes with different biochemical and functional properties. Molecular and cellular biology, *26*, 843-851.

Mizushima, N., B. Levine, A. M. Cuervo and D. J. Klionsky (2008). Autophagy fights disease through cellular self-digestion. nature, *451*, 1069-1075.

Nicolas, G., M. Bennoun, I. Devaux, C. Beaumont, B. Grandchamp, A. Kahn and S. Vaulont (2001). Lack of hepcidin gene expression and severe tissue iron overload in upstream stimulatory factor 2 (USF2) knockout mice. Proceedings of the National Academy of Sciences, *98*, 8780-8785.

Noda, T., N. Sakurai, K. Nozawa, S. Kobayashi, D. J. Devlin, M. M. Matzuk and M. Ikawa (2019). Nine genes abundantly expressed in the epididymis are not essential for male fecundity in mice. Andrology, *7*, 644-653.

Pajukanta, P., H. E. Lilja, J. S. Sinsheimer, R. M. Cantor, A. J. Lusis, M. Gentile, X. J. Duan, A. Soro-Paavonen, J. Naukkarinen and J. Saarela (2004). Familial combined hyperlipidemia is associated with upstream transcription factor 1 (USF1). Nature genetics, *36*, 371-376.

Parenti, G., G. Andria and A. Ballabio (2015). Lysosomal storage diseases: from pathophysiology to therapy. Annual review of medicine, *66*, 471-486.

Pastore, N., K. Blomenkamp, F. Annunziata, P. Piccolo, P. Mithbaokar, R. Maria Sepe, F. Vetrini, D. Palmer, P. Ng and E. Polishchuk (2013). Gene transfer of master autophagy regulator TFEB results in clearance of toxic protein and correction of hepatic disease in alpha-1-anti-trypsin deficiency. EMBO molecular medicine, *5*, 397-412.

Piitulainen, E., J. Carlson, K. Ohlsson and T. Sveger (2005). α1-antitrypsin deficiency in 26-year-old subjects: lung, liver, and protease/protease inhibitor studies. Chest, *128*, 2076-2081.

Platt, F. M., A. d'Azzo, B. L. Davidson, E. F. Neufeld and C. J. Tifft (2018). Lysosomal storage diseases. Nature reviews Disease primers, *4*, 27.

Qu, D., J. H. Teckman, S. Omura and D. H. Perlmutter (1996). Degradation of a mutant secretory protein, α1-antitrypsin Z, in the endoplasmic reticulum requires proteasome activity. Journal of Biological Chemistry, *271*, 22791-22795.

Reynolds, N., M. Salmon-Divon, H. Dvinge, A. Hynes-Allen, G. Balasooriya, D. Leaford, A. Behrens, P. Bertone and B. Hendrich (2012). NuRD-mediated deacetylation of H3K27 facilitates recruitment of Polycomb Repressive Complex 2 to direct gene repression. The EMBO journal, *31*, 593-605.

Rother, M. B. and H. van Attikum (2017). DNA repair goes hip-hop: SMARCA and CHD chromatin remodellers join the break dance. Philosophical Transactions of the Royal Society B: Biological Sciences, *372*, 20160285.

Sakamaki, J.-i., S. Wilkinson, M. Hahn, N. Tasdemir, J. O'Prey, W. Clark, A. Hedley, C. Nixon, J. S. Long and M. New (2017). Bromodomain protein BRD4 is a transcriptional repressor of autophagy and lysosomal function. Molecular cell, *66*, 517-532. e519.

Sayasith, K., J. G. Lussier and J. Sirois (2005). Role of upstream stimulatory factor phosphorylation in the regulation of the prostaglandin G/H synthase-2 promoter in granulosa cells. Journal of Biological Chemistry, *280*, 28885-28893.

Seok, S., T. Fu, S.-E. Choi, Y. Li, R. Zhu, S. Kumar, X. Sun, G. Yoon, Y. Kang and W.

Zhong (2014). Transcriptional regulation of autophagy by an FXR–CREB axis. Nature, *516*, 108-111.

Settembre, C., C. Di Malta, V. A. Polito, M. G. Arencibia, F. Vetrini, S. Erdin, S. U. Erdin, T. Huynh, D. Medina and P. Colella (2011). TFEB links autophagy to lysosomal biogenesis. science, *332*, 1429-1433.

Shin, H.-J. R., H. Kim, S. Oh, J.-G. Lee, M. Kee, H.-J. Ko, M.-N. Kweon, K.-J. Won and S. H. Baek (2016). AMPK–SKP2–CARM1 signalling cascade in transcriptional regulation of autophagy. Nature, *534*, 553-557.

Sirito, M., Q. Lin, J. M. Deng, R. R. Behringer and M. Sawadogo (1998). Overlapping roles and asymmetrical cross-regulation of the USF proteins in mice. Proceedings of the National Academy of Sciences, *95*, 3758-3763.

Spruijt, C. G., M. S. Luijsterburg, R. Menafra, R. G. Lindeboom, P. W. Jansen, R. R. Edupuganti, M. P. Baltissen, W. W. Wiegant, M. C. Voelker-Albert and F. Matarese (2016). ZMYND8 co-localizes with NuRD on target genes and regulates poly (ADP-ribose)-dependent recruitment of GATAD2A/NuRD to sites of DNA damage. Cell reports, *17*, 783-798.

Sveger, T. (1976). Liver disease in alpha1-antitrypsin deficiency detected by screening of 200,000 infants. New England Journal of Medicine, *294*, 1316-1321.

Sveger, T. (1988). The Natural History of Liver Disease in (α1-Antitrypsin Deficient Children. Acta Pædiatrica, *77*, 847-851.

Teckman, J. H. and D. H. Perlmutter (2000). Retention of mutant α1-antitrypsin Z in endoplasmic reticulum is associated with an autophagic response. American Journal of

Physiology-Gastrointestinal and Liver Physiology, *279*, G961-G974.

Torchy, M. P., A. Hamiche and B. P. Klaholz (2015). Structure and function insights into the NuRD chromatin remodeling complex. Cellular and Molecular Life Sciences, *72*, 2491-2507.

Wang, D. and H. S. Sul (1995). Upstream stimulatory factors bind to insulin response sequence of the fatty acid synthase promoter USF1 is regulated. Journal of Biological Chemistry, *270*, 28716-28722.

국문 초록 / ABSTRACT IN KOREAN

오토파지는 세포 항상성을 유지하는 데 중요한 고도로 보존된 자가소화 과정으로, 영양 결핍을 포함한 다양한 환경 신호에 의해 유도된다. 리소좀 및 오토파지 관련 과정의 조절은 세포 항상성과 기초 대사 유지에 필수적이다. 리소좀 및 오토파지 시스템이 방해되거나 감소될 경우의 결과는 많이 연구되었으나, 리소좀 및 오토파지 유전자 과활성화가 항상성에 미치는 영향에 대한 정보는 제한적이다.

이 연구에서는 영양이 풍부한 조건에서 리소좀 및 오토파지 유전자를 억제하는 전사 억제 메커니즘을 제시하며, 이는 Upstream Stimulatory Factor 2 (USF2)를 포함한다. USF2는 HDAC1과 함께 리소좀 유전자의 CLEAR 모티프에 결합하여 히스톤 H3K27 아세틸화를 감소시키고, 크로마틴 접근성을 제한하며, 리소좀 유전자 발현을 억제하는 것으로 나타났다. 영양 결핍 상태에서는 USF2가 리소좀 및 오토파지 유전자의 주된 전사 활성화자인 TFEB와 경쟁적으로 타겟 유전자 프로모터에 결합하며, 이는 인산화 의존적 방식으로 이루어진다. USF2의 S155 부위에서의 GSK3β 매개 인산화는 USF2의 DNA 결합 활성을 조절하며, 리소좀 유전자 억제에 관여한다. 이러한 연구 결과는 α1-항트립신 결핍증과 같은 단백질 응집 관련 질환 치료에 잠재적인 적용 가능성을 제공한다. 특히, USF2 억제는 리소좀 및 오토파지 관련 질환에 대한 유망한 치료 전략으로 주목된다.

주요어:

Upstream Stimulatory Factor 2 (USF2), Nucleosome Remodeling and Deacetylation

(NuRD), **오토파지** (**자가포식**), **히스톤 아세틸화**, Transcription factor EB (TFEB), a1-AntiTrypsin Deficiency (AATD)

학번: 2016-20380